International Journal of Mechanical Sciences 145 (2018) 330–345

Contents lists available at ScienceDirect

International Journal of Mechanical Sciences

journal homepage: www.elsevier.com/locate/ijmecsci

Comparison of inverse identification strategies for constitutive mechanical models using full-field measurements

J.M.P. Martins[a,b,*], A. Andrade-Campos[a], S. Thuillier[b]

[a] Centre for Mechanical Technology and Automation (TEMA), GRIDS Research Unit, Mechanical Engineering Department, University of Aveiro, Portugal
[b] Univ. Bretagne Sud, UMR CNRS 6027, Lorient, IRDL F-56100, France

ARTICLE INFO

MSC:
00-01
99-00

Keywords:
Parameter identification
Inverse problem
Full-field measurements
Finite element method
Linear elasticity
Elasto-plasticity

ABSTRACT

The calibration of phenomenological constitutive material models has been a constant need, because the parameters differ for each material and the ability of a model to mimic the real behaviour of a material is highly dependent on the quality of these parameters. Classically, the parameters of constitutive models are determined by standard tests under the assumption of homogeneous strain and stress fields in the zone of interest. However, in the last decade, Digital Image Correlation techniques and full-field measurements have enabled the development of new parameter identification strategies, such as the Finite Element Model Updating, the Constitutive Equation Gap Method, the Equilibrium Gap Method and the Virtual Fields Method. Although these new strategies have proven to be effective for linear and non-linear models, the implementation procedure for some of them is still a laborious task. The aim of this work is to give a detailed insight into the implementation aspects and validation of these methods. Detailed flowcharts of each strategy, focusing on the implementation aspects, are presented and their advantages and disadvantages are discussed. Moreover, these modern strategies are compared for the cases of homogeneous isotropic linear elasticity and isotropic plasticity with isotropic hardening. A simple numerical example is used to validate and compare the different strategies.

1. Introduction

With the innovation surge currently happening in industry, reliable and fast solutions for engineering problems are more important than ever. Numerical simulation has been a valuable tool for their resolution and is now well-established. However, it is essential for these tools to keep a continuous improvement of their predictive capabilities. One of the areas for potential improvement is mechanical modelling of materials and the respective calibration procedure. The quest for more accurate models has been particularly intense regarding the elasto-plastic behaviour of sheet metals. Indeed, many advanced and more complex mechanical models have been developed to accurately describe phenomena such as hardening and anisotropy. However, this increase in complexity usually means a tedious process of parameter calibration, due to long experimental campaigns. For example, the yield criterion Yld2000 [1] depends on 8 material parameters, which requires three uniaxial yield stresses and three uniaxial anisotropy coefficients, the biaxial yield stress and anisotropy coefficient. Consequently, in industrial practice, simpler models are still preferred to avoid such experimental campaign and complex identification process [2]. Therefore, there is a clear demand for new processes of calibration that can simplify the experimental campaign without compromising the accuracy of the models.

Nowadays, there are two main approaches to conduct the identification process: a classical approach and a more recent one based on full-field measurements [3,4]. The classical approach relies on simple tests, that provide near homogeneous strain and stress states over the zone of interest. It is taken advantage of this homogeneity to retrieve the material parameters from simple analytical solutions. This kind of approach has several drawbacks, i.e.: (i) the limited exploitation of experimental tests, since homogeneous stress and strain state assumption can no longer be used after the onset of necking; (ii) the large number of tests required when complex constitutive models have to be calibrated; and (iii) the stress and strain fields do not resemble the ones obtained in forming operations.

The second approach is increasingly being used, mainly because of the rapid development of full-field measurements techniques, such as digital image correlation [5]. These techniques allow a more flexible design of mechanical tests and take advantage of the heterogeneous displacement/strain fields [6]. Indeed, due to the heterogeneity, each material point experiences a different stress and strain history, hence the

* Corresponding author at: Centre for Mechanical Technology and Automation (TEMA), GRIDS Research Unit, Mechanical Engineering Department, University of Aveiro, Portugal.
E-mail addresses: joao.martins52@ua.pt (J.M.P. Martins), gilac@ua.pt (A. Andrade-Campos), sandrine.thuillier@univ-ubs.fr (S. Thuillier).

https://doi.org/10.1016/j.ijmecsci.2018.07.013
Received 20 February 2018; Received in revised form 11 July 2018; Accepted 14 July 2018
Available online 19 July 2018
0020-7403/© 2018 Elsevier Ltd. All rights reserved.

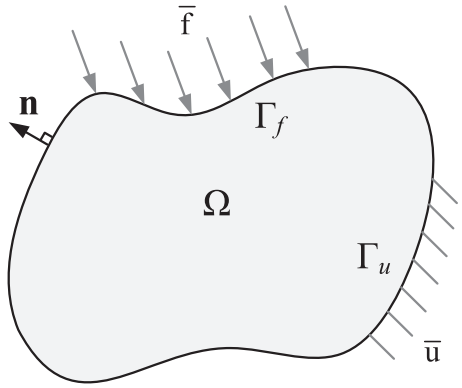

Fig. 1. Domain Ω with prescribed displacement and traction boundary conditions.

number of material parameters governing the field is generally greater than those driving homogenous strain fields [7]. Therefore, this second approach enables to reduce the number of experiments required to calibrate a model. Furthermore, it enables to extend the exploitation limits of a test, since the heterogeneous fields are no longer a problem. However, effective inverse strategies to extract the material parameters from full-field measurements are required.

Accordingly, the development of inverse strategies in computational mechanics has evolved rapidly in recent years, leading to an interesting number of strategies based on full-field measurements, e.g. [3,4,8,9]. The most well-known methods are the Finite Element Model Updating (FEMU) [10], the Constitutive Equation Gap Method (CEGM) [11], the Equilibrium Gap Method (EGM) [12,13] and the Virtual Fields Method (VFM) [14]. These four strategies prove to be effective in identifying parameters associated with linear and non-linear models and, therefore, these will be the focus of this work. However, it should also be mentioned that more strategies have emerged recently with promising results, such as the Constitutive Compatibility Method (CCM) [15], the Dissipation Gap Method [16], the Self-Optimizing Method (Self-OPTIM) [17] and the Integrated Digital Image Correlation Method (Integrated-DIC) [18].

To the best of the authors knowledge, studies on the implementation aspects of these strategies, as well as comparative studies, are rare, specially in elasto-plasticity. Since the mentioned strategies rely on different principles, it is interesting to evaluate their performance in the same conditions, as well as their sensitivity to noise. Thus, the aim of this study is to introduce the four strategies mentioned above, discuss the implementation details and finally, present a comparative study for quasi-static loading conditions. For the sake of simplicity, the scope of this study lies within the framework of infinitesimal small strains. The extension to large strains can be tedious [19,20], with the exception of FEMU, and is out of the scope of this article.

The outline of this work is as follows. A brief description of the inverse problem and the constitutive models used in this study is presented in Section 2. The four inverse strategies selected, FEMU, CEGM, EGM and VFM, are presented in Section 3, as well as flowcharts for each one and a discussion of the main advantages and drawbacks. Finally, in Section 4, the performance of these strategies is compared for two different constitutive models. This performance study starts with a simple case of an isotropic linear elastic model that is afterwards extended for an elasto-plastic model with isotropic non-linear hardening. Moreover, the comparative studies are performed with and without noise.

2. Identification/inverse problem

Consider a continuum solid body whose reference configuration occupies the domain Ω and is bounded by $\partial\Omega$ (see Fig. 1). It is assumed that the material within the domain Ω is homogeneous. The boundary of this body is composed of two sub-boundaries Γ_f and Γ_u, such that $\partial\Omega = \Gamma_f \cup \Gamma_u$ and $\Gamma_f \cap \Gamma_u = \emptyset$. A surface external force is prescribed over Γ_f, possibly with a null value, and a displacement field is prescribed over Γ_u. Neglecting the body forces and assuming static equilibrium, a linear elastic behaviour and infinitesimally small displacements, the mechanical state of the body is governed by three sets of equations: the equilibrium equations,

$$\begin{cases} \mathrm{div}\boldsymbol{\sigma} = 0 & \text{in } \Omega, \\ \boldsymbol{\sigma}\cdot\mathbf{n} = \bar{\mathbf{f}} & \text{on } \Gamma_f, \end{cases} \tag{1}$$

the kinematic compatibility equations,

$$\begin{cases} \boldsymbol{\varepsilon} = \frac{1}{2}\left(\nabla\mathbf{u}(\mathbf{x}) + \nabla^{\mathrm{T}}\mathbf{u}(\mathbf{x})\right) & \text{in } \Omega, \\ \mathbf{u} = \bar{\mathbf{u}} & \text{on } \Gamma_u, \end{cases} \tag{2}$$

and the constitutive equation,

$$\boldsymbol{\sigma} = \mathbf{C} : \boldsymbol{\varepsilon} \qquad \text{in } \Omega, \tag{3}$$

where $\boldsymbol{\sigma}$ denotes the Cauchy stress tensor, $\bar{\mathbf{f}}$ is the prescribed vector of external forces over Γ_f, $\mathbf{u}$ is the displacement vector field, $\bar{\mathbf{u}}$ is the prescribed displacement vector field over Γ_u, $\boldsymbol{\varepsilon}$ is the infinitesimal strain tensor and $\mathbf{n}$ the unit normal vector to $\partial\Omega$.

The stress and strain are related through Eq. (3), for which $\mathbf{C}$ is the constitutive material tensor. It is assumed to be function of a vector that gathers all the unknown constitutive material parameters $\boldsymbol{\xi} = \{\xi_1, \dots, \xi_n\}$ (n is the number of material parameters). In case of isotropic linear elastic behaviour, $\mathbf{C}(\boldsymbol{\xi})$ represents the Hooke's elasticity tensor and $\boldsymbol{\xi}$ contains two parameters: Poisson's ratio ν and Young's modulus E, $\boldsymbol{\xi} = \{\nu, E\}$, respectively.

For the direct problem of continuum mechanics, the initial shape of the solid body, the material parameters and the set of boundary conditions, $\bar{\mathbf{f}}$ and $\bar{\mathbf{u}}$, are assumed to be known. Accordingly, the unknowns are the fields $(\mathbf{u}, \boldsymbol{\varepsilon}, \boldsymbol{\sigma})$, which must satisfy the three previous sets of Eqs. (1), (2) and (3). For the inverse problem of parameter identification using full-field measurements, the aim is to retrieve the material parameters given a discrete observation of the displacement field $\hat{\mathbf{u}}$ and information concerning the boundary conditions, $\bar{\mathbf{f}}$ and $\bar{\mathbf{u}}$. The measured displacement field $\hat{\mathbf{u}}$ can be obtained, for instance, through a non-contact measurement technique, such as DIC, and the strain field required to calculate the stress field can be calculated using Eq. (2). The idea behind the inverse problem is to explore an implicit relationship between the measured displacement field and the parameters of the constitutive model.

Typically, full-field measurements are performed on the surface of the body and this limits the identification through the volume. Therefore, the inverse problem in linear and non-linear cases is usually seen as a in-plane problem, for which the plane stress assumption can be adopted. This assumption implies that the body with domain Ω is a thin flat body, with volume V and a constant thickness t that is assumed much smaller than the other dimensions. Furthermore, the body only undergoes in-plane loading.

For the case of non-linear elasto-plastic behaviour, the linear relationship between stress and strain is no longer valid, and the constitutive equations are obtained within the classical incremental theory of plasticity. In the following, these equations are briefly recalled.

Consider the additive decomposition of the total strain tensor increment $d\boldsymbol{\varepsilon}$, in terms of elastic $d\boldsymbol{\varepsilon}^{\mathrm{e}}$ and plastic $d\boldsymbol{\varepsilon}^{\mathrm{p}}$ components, which can be written as

$$d\boldsymbol{\varepsilon} = d\boldsymbol{\varepsilon}^{\mathrm{e}} + d\boldsymbol{\varepsilon}^{\mathrm{p}}. \tag{4}$$

Moreover, consider an hypoelastic relationship to describe the stress-strain relation, as follows

$$d\boldsymbol{\sigma} = \mathbf{C} : \left(d\boldsymbol{\varepsilon} - d\boldsymbol{\varepsilon}^{\mathrm{p}}\right), \tag{5}$$

where $d\boldsymbol{\sigma}$ is the stress increment. The plastic strain increment $d\boldsymbol{\varepsilon}^{\mathrm{p}}$ can be defined by means of three key concepts: a yield criterion, a hardening

law and a plastic flow rule. The von Mises yield criterion is adopted here, thus the yield condition can be expressed as

$$f(\boldsymbol{\sigma}, \bar{\varepsilon}^{\mathrm{p}}) = \bar{\sigma}(\boldsymbol{\sigma}) - \sigma_y\left(\bar{\varepsilon}^{\mathrm{p}}\right) = 0, \tag{6}$$

where $\sigma_y(\bar{\varepsilon}^{\mathrm{p}})$ is the yield stress as a function of the equivalent plastic strain $\bar{\varepsilon}^{\mathrm{p}}$ and $\bar{\sigma}(\boldsymbol{\sigma})$ is the equivalent von Mises stress, which under plane stress conditions assumes the following form

$$\bar{\sigma}(\boldsymbol{\sigma}) = \sqrt{\frac{3}{2}\boldsymbol{\sigma}'(\boldsymbol{\sigma}) : \boldsymbol{\sigma}'(\boldsymbol{\sigma})} = \sqrt{\sigma_{xx}^2 + \sigma_{yy}^2 - \sigma_{xx}\sigma_{yy} + 3\sigma_{xy}^2}, \tag{7}$$

where $\boldsymbol{\sigma}'(\boldsymbol{\sigma})$ is the deviatoric stress tensor and σ_{xx}, σ_{yy} and σ_{xy} are the components of the stress tensor. The evolution of the yield stress is governed by the Swift's isotropic hardening law, with the following form

$$\sigma_y\left(\bar{\varepsilon}^{\mathrm{p}}\right) = K\left(\varepsilon_0 + \bar{\varepsilon}^{\mathrm{p}}\right)^n, \tag{8}$$

which depends on three material parameters, K, ε_0 and n.

The classical associated flow rule is adopted, which can be introduced as

$$d\boldsymbol{\varepsilon}^{\mathrm{p}} = d\lambda\frac{\partial f}{\partial \boldsymbol{\sigma}}, \tag{9}$$

it defines the plastic strain increment. The direction of the plastic flow is defined by the term $\partial f/\partial\boldsymbol{\sigma}$ and the magnitude is given by the plastic multiplier $d\lambda$. Based on this, Eq. (5), which gives the stress increment, can be updated to

$$d\boldsymbol{\sigma} = \mathbf{C} : \left(d\boldsymbol{\varepsilon} - d\lambda\frac{\partial f}{\partial \boldsymbol{\sigma}}\right). \tag{10}$$

For the von Mises yield criterion, the plastic multiplier is equivalent to the increment in the equivalent plastic strain $d\bar{\varepsilon}^{\mathrm{p}}$ [21], which is defined as

$$d\bar{\varepsilon}^{\mathrm{p}} = \sqrt{\frac{2}{3}d\boldsymbol{\varepsilon}^{\mathrm{p}} : d\boldsymbol{\varepsilon}^{\mathrm{p}}}. \tag{11}$$

The plastic multiplier is explicitly determined using the consistency condition, which imposes that the current stress state remains on the yield surface after yielding and can be written as

$$df = \frac{\partial f}{\partial \boldsymbol{\sigma}} : d\boldsymbol{\sigma} + \frac{\partial f}{\partial \bar{\varepsilon}^{\mathrm{p}}} : d\bar{\varepsilon}^{\mathrm{p}} = 0. \tag{12}$$

By replacing the stress increment (Eq. (10)) in the consistency condition (Eq. (12)) and after some algebra manipulation, the plastic increment can be explicitly obtained:

$$d\lambda = \frac{\frac{\partial f}{\partial \boldsymbol{\sigma}} : \mathbf{C} : d\boldsymbol{\varepsilon}}{\frac{\partial f}{\partial \boldsymbol{\sigma}} : \mathbf{C} : \frac{\partial f}{\partial \boldsymbol{\sigma}} - \frac{\partial f}{\partial \bar{\varepsilon}^{\mathrm{p}}}\sqrt{\frac{2}{3}\frac{\partial f}{\partial \boldsymbol{\sigma}} : \frac{\partial f}{\partial \boldsymbol{\sigma}}}} \tag{13}$$

Finally, Eq. (10) for the stress increment can be updated and gives

$$d\boldsymbol{\sigma} = \left(\mathbf{C} - \frac{\frac{\partial f}{\partial \boldsymbol{\sigma}} : \mathbf{C} \otimes \mathbf{C} : \frac{\partial f}{\partial \boldsymbol{\sigma}}}{\frac{\partial f}{\partial \boldsymbol{\sigma}} : \mathbf{C} : \frac{\partial f}{\partial \boldsymbol{\sigma}} - \frac{\partial f}{\partial \bar{\varepsilon}^{\mathrm{p}}}\sqrt{\frac{2}{3}\frac{\partial f}{\partial \boldsymbol{\sigma}} : \frac{\partial f}{\partial \boldsymbol{\sigma}}}}\right) : d\boldsymbol{\varepsilon} \tag{14}$$

or

$$d\boldsymbol{\sigma} = \mathbf{C}^{\mathrm{ep}} : d\boldsymbol{\varepsilon}, \tag{15}$$

where $\mathbf{C}^{\mathrm{ep}}$ is the so-called elasto-plastic tangent stiffness matrix. This matrix is a function of the unknown material parameters, so it can be defined as function of the material parameters $\mathbf{C}^{\mathrm{ep}}(\boldsymbol{\xi})$. For this elasto-plastic model, the material parameters vector gathers five parameters $\boldsymbol{\xi} = \{\nu, E, K, \varepsilon_0, n\}$.

In this case, the inverse problem must take into account the history dependent behaviour of plasticity. Therefore, deformation history during the experiment must be acquired, which means measurements of displacement field for different time instants $\hat{\mathbf{u}}(\mathbf{x}, t)$ (for which $t \in [0, T]$) must be performed and used to solve the inverse problem. Thus, the total strain is discretized along the time, as well as the boundary conditions.

3. Inverse strategies based on full-field measurements

3.1. Finite element model updating

Among all inverse strategies available for identifying material parameters, Finite Element Model Updating (FEMU) is the most used. Since the introduction of this strategy by Kavanag and Clough [10], a significant number of studies have been published. It was used with a wide range of models, e.g. elasticity [22,23], plasticity with emphasis on sheet metal forming [3,24–26] and viscoplasticity [27,28].

The idea behind this strategy is to infer the unknown material parameters after comparing numerical predictions with experimental measurements. Therefore, it requires a finite element (FE) model of the mechanical test, to generate numerical predictions of the response of the material. Based on the comparison between experimental and numerical data and by means of an optimization method, the material parameters are adjusted iteratively until the numerical results match the experimental ones as closely as possible.

The data used with this strategy can be of different kinds: displacements, strains, force, temperatures, etc. FEMU is easily adapted to the available experimental data. In fact, it is not mandatory to use full-field measurements with FEMU, partial measurements of the complete field can also be used. The choice of the data has been a widely discussed subject on this strategy and the literature reveals a lack of consensus [3]. Another widely discussed point is how the experimental data are compared with the numerical data. This comparison is usually performed using an objective function that evaluates the gap between experimental and numerical results. However, this objective function can assume different formulations [29,30]. An example of an objective function based on the measured strains on the surface of the sample can be defined as

$$\mathcal{F}_{\mathrm{FEMU}}(\boldsymbol{\xi}) = \sum_{i=1}^{n_{\mathrm{s}}}\sum_{j=1}^{n_{\mathrm{p}}}\left[\left(\hat{\varepsilon}_{xx} - \varepsilon_{xx}(\boldsymbol{\xi})\right)_j^2 + \left(\hat{\varepsilon}_{yy} - \varepsilon_{yy}(\boldsymbol{\xi})\right)_j^2 + \left(\hat{\varepsilon}_{xy} - \varepsilon_{xy}(\boldsymbol{\xi})\right)_j^2\right]_i. \tag{16}$$

This objective function is formulated based on the sum of the squares of the gap between experimental $(\hat{\varepsilon}_{xx}, \hat{\varepsilon}_{yy}, \hat{\varepsilon}_{xy})$ and numerical (ε_{xx}, ε_{yy}, ε_{xy}) data, considering the different components of the in-plane strain tensor. The experimental data (full strain field) are usually made of a discrete number of values representing the measurement points on the surface of the sample for different time instants ($\hat{\varepsilon}(\mathbf{x}, t)$). The variables n_{p} and n_{s}, in Eq. (16), represent the number of measurement points on the surface of the sample and the number of time instants for which measurements are performed, respectively.

It is a common practice to use weighting coefficients in the formulation of the objective function (e.g. [31]), but their selection is not intuitive and usually depends on the user [30]. Therefore, the use of weights will be avoided in this work.

Another important remark regarding the evaluation of the objective function is that the numerical data must be calculated at the exact same locations as the experimental points. Otherwise, the numerical data must be interpolated to match these locations.

A detailed flowchart for FEMU strategy is presented in Fig. 2. In the flowchart, B.C. stands for boundary conditions. It starts with an initial set of material parameters ($\boldsymbol{\xi}^{\mathrm{i}}$) arbitrarily chosen used to run the first FE analysis. The evaluation of the objective function is then performed. If the value of the objective function is above a threshold value, the iterative process starts and the optimization method generates a new (or updated) set of material parameters ($\boldsymbol{\xi}^{\mathrm{u}}$). The process is repeated until the value of the objective function reaches a value below the threshold or until the set of parameters stagnates. The threshold value is defined by the user and represents the admissible global gap between numerical and experimental results.

Within the iterative cycle of FEMU, the update of the material parameters is performed by searching for a minimum in the objective func-

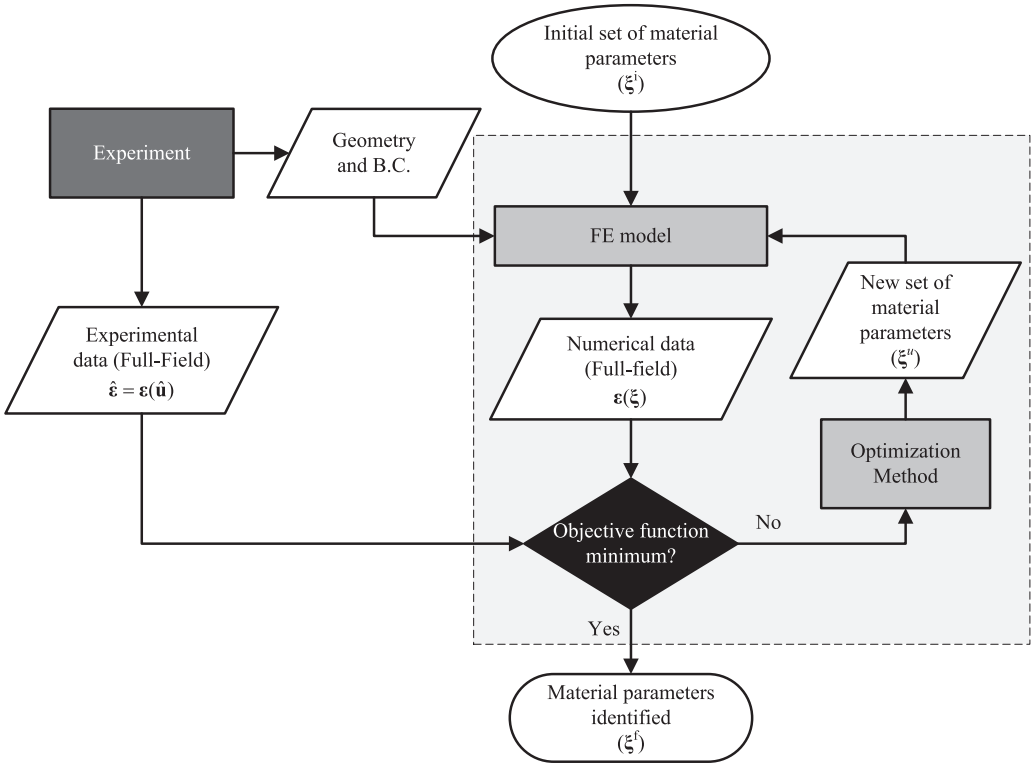

Fig. 2. Detailed flowchart for the FEMU.

tion. Coupling an optimization method with the objective function is the usual way to do it. The type of optimization methods used in this kind of problem lies within two main families: (i) the gradient-based methods (e.g. the Gauss-Newton method or the Levenberg–Marquardt method) and (ii) the direct methods (e.g. evolutionary and simplex) [3,30,32]. The first family of methods is the most used. It requires the value of the objective function and its gradient to take a decision, whereas the direct methods only use the value of the objective function. The use of gradient-based methods is related to its computational efficiency, since they usually require less evaluations of the objective function. However, this type of methods has a major disadvantage. They do not guarantee the location of the global minimum and depend on the initial set of material parameters chosen to initiate the identification procedure [25]. Other methods that will be described also require the coupling with optimization methods, so whenever invoked in the context of other methods the reader can review this section.

As mentioned before, FEMU is not limited to full-field measurements, which gives an even wider range of applications. Another important feature of FEMU is that it can be adapted to complex specimen shapes and loads. For instance, a curved sample cut from a coil steel [33]. These advantages and the ease of the implementation make FEMU very attractive. However, the major drawback that has been pointed out over the years and that motivated researchers to develop other strategies is the excessive computational cost (e.g. [34]), consequence of the FE analysis at each evaluation of the objective function. In addition, the analysis requires a FE model that represents the experimental test as close as possible to reality, which can be difficult to attain depending on the geometry and load conditions. However, it is strictly necessary to avoid undesired errors. Moreover, the results can also be mesh sensitive, which is an aspect inherent to every method that makes use of FE analysis.

3.2. Constitutive equation gap method

The Constitutive Equation Gap Method (CEGM) (also called as, Error in the Constitutive Equation) was first proposed by Ladevèze and Leguillon [11], as an error estimation procedure for FE analysis. It was applied in a variety of fields [35,36], before being adapted to identify material parameters of an elastic isotropic model based on full-field measurements [37], with significant efforts for heterogeneous materials [38,39]. More recently, Guchhait and Banerjee [40] extended it for anisotropic elasticity. Moreover, it has also been used in the field of plasticity [41] and damage [42].

CEGM objective function is based on the evaluation of the error between a statically admissible stress field, denoted $\boldsymbol{\tau}$, and a stress field calculated from a measured displacement/strain field $\hat{\boldsymbol{\varepsilon}} = \boldsymbol{\varepsilon}(\hat{\mathbf{u}})$ and a chosen constitutive model. This error is quantified by means of an energy norm. In the case of linear elasticity, it leads to the following objective function

$$\mathcal{F}_{\mathrm{CEGM}}(\boldsymbol{\tau}, \boldsymbol{\xi}) = \frac{1}{2}\int_{\Omega} [\boldsymbol{\tau} - \mathbf{C}(\boldsymbol{\xi}) : \hat{\boldsymbol{\varepsilon}}] : \mathbf{C}^{-1}(\boldsymbol{\xi}) : [\boldsymbol{\tau} - \mathbf{C}(\boldsymbol{\xi}) : \hat{\boldsymbol{\varepsilon}}] \mathrm{d}\Omega, \tag{17}$$

If the statically admissible stress field describes correctly the stress state of the body and the material parameters fit the description of the material behaviour, the objective function value should be close to zero.

The flowchart for the CEGM is presented in Fig. 3. The first step is to define an initial set of material parameters (ξ^i), followed by the determination of a statically admissible stress field with this initial set of material parameters. Then, the objective function is evaluated. If its value is above a threshold the optimization method generates a new set of material parameters (ξ^u). This process is repeated until the value of the objective function reaches a value below the threshold or until the process stagnation. After that, the statically admissible stress field is updated. It is updated in accordance with a user-defined criterion and using the new set of material parameters. The whole process is repeated again for the new statically admissible stress field. The convergence criterion for the statically admissible stress field can be checked by comparing the stress in the current and the last iteration [41].

The statically admissible stress field $\boldsymbol{\tau}$ is a key requisite of this strategy. This stress field must verify the force boundary conditions of the experimental test, as well as the equilibrium equation (Eq. (1)). It can be determined, for specific geometries and boundary conditions, by an an-

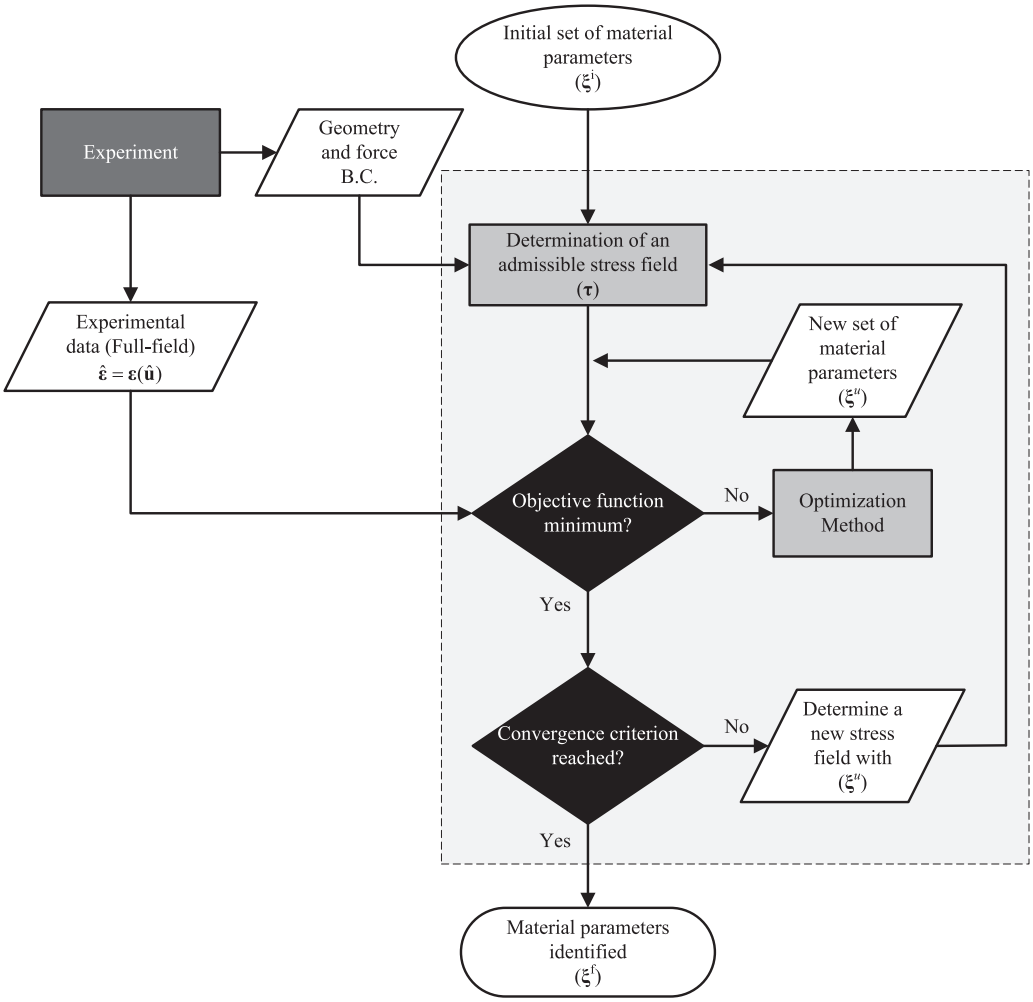

Fig. 3. Detailed flowchart for the CEGM.

alytic solution or, in a more general way, through a FE model [42]. Special techniques have also been developed to determine it when heterogeneous materials are analyzed [38,39]. In the present work, a FE model is adopted and the determination of the statically admissible stress field is performed before the minimization of the objective function (Fig. 3) . Note that, in case of homogeneous materials the admissible stress field is uniquely determined by the force boundary conditions, *i.e.*, it is independent of the material parameters. Therefore, it is not required to update it along the process.

Regarding the implementation of the CEGM, Eq. (17) can be converted into a more practical form which benefits from the discrete nature of experimental measurements acquired, for example, by DIC. In fact, displacements or strain fields are measured in a discrete number of points, which are usually associated with a mesh that results from a non-overlapping decomposition of the surface of the domain Ω. Therefore, each measurement point is representative of a small area or small element in this mesh. Moreover, measurements are acquired for a finite number of time instants during the experimental test. Considering this discrete nature of experimental measurements, the objective function (Eq. (17)) can be rewritten as follows

$$\mathcal{F}_{\mathrm{CEGM}}(\boldsymbol{\tau},\boldsymbol{\xi}) = \frac{1}{2}\sum_{i=1}^{n_s}\left[t\sum_{j=1}^{n_p} A_j \left\{\left[\boldsymbol{\tau}_j - \mathbf{C}(\boldsymbol{\xi}) : \hat{\boldsymbol{\varepsilon}}_j\right] : \mathbf{C}^{-1}(\boldsymbol{\xi}) : \left[\boldsymbol{\tau}_j - \mathbf{C}(\boldsymbol{\xi}) : \hat{\boldsymbol{\varepsilon}}_j\right]\right\}\right]_i , \tag{18}$$

where A_i is the representative area of each measurement point. Eq. (17) is integrated over the volume, but as plane stress conditions are assumed, the stress distribution is considered constant through the thickness t of the body. Note that the same mesh can be used to determine the statically admissible stress field, thus preventing an additional step for interpolation.

Until now CEGM has been described with focus on linear elasticity. Concerning the identification of material parameters for non-linear models, the determination or reconstruction of the stress field from the measured displacement/strain field is more challenging than in linear elasticity, due to the history dependent behaviour. In this case, a stress update algorithm to reconstruct the actual stress field is required. It is a common point with other identification strategies and FE codes, thus, different algorithms have been proposed, e.g. [9,20,43]. Here, considering the assumptions of Section 2 for plane stress elasto-plasticity, it will be adopted an implicit backward-Euler algorithm presented in [44]. This step is included in the evaluation of the objective function, hence the flowchart presented in Fig. 3 is also valid for the non-linear case. However, the objective function (Eq. (17)) assumes a different form, as follows

$$\mathcal{F}_{\mathrm{CEGM}}(\boldsymbol{\tau},\boldsymbol{\xi}) = \sum_{i=1}^{n_s}\left(\frac{1}{2}\int_{\Omega}[\boldsymbol{\tau} - \boldsymbol{\sigma}(\boldsymbol{\xi},\hat{\boldsymbol{\varepsilon}})] : \mathbf{C}^{-1} : [\boldsymbol{\tau} - \boldsymbol{\sigma}(\boldsymbol{\xi},\hat{\boldsymbol{\varepsilon}})]\mathrm{d}\Omega\right)_i . \tag{19}$$

The stress field $\boldsymbol{\sigma}(\boldsymbol{\xi},\hat{\boldsymbol{\varepsilon}})$ is now calculated by the stress update algorithm, taking into account the history dependent behaviour of plasticity. This formulation differs from the ones presented in [41], because it uses the inverse of the elastic stiffness matrix instead of the elasto-plastic tangent/secant stiffness matrices. This kind of formulation can be used when elastic material parameters are known *a priori*.

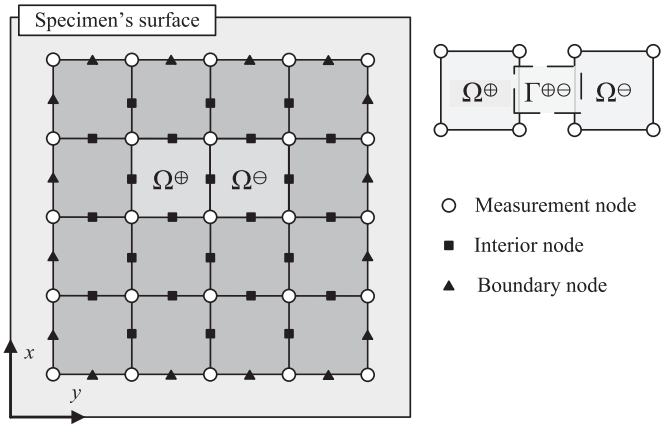

Fig. 4. Specimen's surface and measurement grid with the localization of the calculation points (adapted from [38]).

Regarding the advantages of CEGM, it can be applied to any constitutive model, although proper algorithms must be implemented to reconstruct the stress field from the measured data. Moreover, as FEMU, it is not restricted to full-field measurements [32]. The major drawback of CEGM is the calculation of a statically admissible stress field. It can be a laborious task, particularly when a heterogeneous distribution of the material properties is considered. When a FE model is used to generate this stress field, CEGM is affected by the same drawbacks related to the construction of a FE model. Compared with FEMU, it requires a lower number of simulations. Consequently, in terms of computational cost, CEGM is more efficient than FEMU. However, the implementation of the algorithm (Fig. 3) is not so intuitive as the one of FEMU (Fig. 2).

3.3. Equilibrium gap method

The Equilibrium Gap Method (EGM) was first proposed by Claire et al. [12,13] with the aim of identifying isotropic damage fields in heterogeneous materials resorting only to full-field measurements (the force boundary conditions were not taken into account). In this first attempt, the degradation of the elastic stiffness depended on a damage scalar variable [12,13]. Roux and Hild extended this method to more complex damage laws [45]. Later, Périé et al. [46] have proposed the extension of EGM to anisotropic damage. Moreover, Florentin and Lublineau [38] have used EGM as a reference to compare with CEGM in the identification of isotropic elastic parameters in heterogeneous materials. Although it has not yet been extended to elasto-plasticity, it could be performed by means of a method that captures the history dependent behaviour of non-linear models [45].

The implementation of the EGM can be performed following two different frameworks: finite-difference or finite element based formulations [47]. In this work, it is adopted a finite-difference version inspired from [38], which is adapted to homogeneous isotropic material behaviour.

To better describe the EGM, consider that the surface of a specimen is discretized in small subdomains that represent a measurement grid, as shown in Fig. 4. It is assumed that the experimental strain field ($\hat{\boldsymbol{\varepsilon}} = \boldsymbol{\varepsilon}(\hat{\mathbf{u}})$) is provided at the nodes of each subdomain (circles in Fig. 4). The EGM consists on the minimization of the gap in local equilibrium on the boundaries of each subdomain. The local equilibrium is expressed by assessing the continuity of the stress vector at the interfaces. For instance, considering the two subdomains $\Omega^{\oplus}$ and $\Omega^{\ominus}$ represented in Fig. 4, the local equilibrium for the boundary $\Gamma^{\oplus\ominus}$ can be expressed as

$$\boldsymbol{\sigma}^{\oplus} \cdot \mathbf{n}^{\oplus} + \boldsymbol{\sigma}^{\ominus} \cdot \mathbf{n}^{\ominus} = \mathbf{0}, \tag{20}$$

where $\mathbf{n}^{\oplus}$ and $\mathbf{n}^{\ominus}$ are the unit normal vectors to the boundaries of $\Omega^{\oplus}$ and $\Omega^{\ominus}$, respectively. $\mathbf{0}$ is the zero vector. For the elasticity case, $\boldsymbol{\sigma}^{\oplus}$ and $\boldsymbol{\sigma}^{\ominus}$ are calculated with Eq. (3) and the given measured strain field. Note that Eq. (20) results in two equations for each interface, one for each direction x and y.

A key point is that the strain measurements must be interpolated for the locations where the equilibrium is prescribed, i.e. the interfaces of the subdomains. In Fig. 4, the interface of each subdomain is marked with triangular and quadrangular marks. The interpolation can be performed using finite element shape functions [38].

In case of a boundary where a force boundary condition $\bar{\mathbf{f}}$ is prescribed, the equilibrium is prescribed as

$$\boldsymbol{\sigma} \cdot \mathbf{n} = \bar{\mathbf{f}}. \tag{21}$$

This condition can be difficult to impose since the distribution of the force needs to be known. However, there are other ways to verify the local equilibrium that, for example, make use of a weak form of Eq. (21). The weak form allows to use the resultant of the force $\bar{\mathbf{f}}$, but the left-hand side of Eq. (21) must be integrated over the boundary Γ_f [47].

In case of a free boundary, the force boundary condition is equal to zero ($\bar{\mathbf{f}} = \mathbf{0}$). For the boundaries with prescribed displacements (the imposed force is unknown), the stress vector continuity cannot be evaluated, hence these boundaries are not taken into account. Finally, the objective function can be written in a least-square based formulation, as follows

$$\mathcal{F}_{\mathrm{EGM}}(\boldsymbol{\xi}) = \sum_{i=1}^{n_{\mathrm{s}}} \left[\sum_{j=1}^{n_{\mathrm{d}}} \left\{ \left(\boldsymbol{\sigma}^{\oplus} \cdot \mathbf{n}^{\oplus} + \boldsymbol{\sigma}^{\ominus} \cdot \mathbf{n}^{\ominus}\right)_j \cdot \left(\boldsymbol{\sigma}^{\oplus} \cdot \mathbf{n}^{\oplus} + \boldsymbol{\sigma}^{\ominus} \cdot \mathbf{n}^{\ominus}\right)_j \right\} \right]_i + \sum_{i=1}^{n_{\mathrm{s}}} \left[\sum_{i=1}^{n_{\mathrm{b}}} \left\{ (\boldsymbol{\sigma} \cdot \mathbf{n} - \bar{\mathbf{f}})_j \cdot (\boldsymbol{\sigma} \cdot \mathbf{n} - \bar{\mathbf{f}})_j \right\} \right]_i, \tag{22}$$

where n_{d} and n_{b} are the number of interface/interior nodes within the domain Ω and at the boundary Γ, respectively.

Fig. 5 shows a flowchart for this strategy. The algorithm starts with an initial set of material parameters ($\boldsymbol{\xi}^{\mathrm{i}}$) that can be arbitrarily chosen. Follows the interpolation of the strain field to the interface boundaries of each subdomain, which can be performed using finite element shape functions. Then, the equilibrium equations are written for each boundary and the objective function is evaluated. In case of reaching a minimum value of the objective function or the process stagnation, the algorithm is interrupted and the set of material parameters ($\boldsymbol{\xi}^{\mathrm{f}}$) is determined. Otherwise, a new iteration is initiated and, by means of an optimization method, a new set of material parameters ($\boldsymbol{\xi}^{\mathrm{u}}$) is determined.

Unlike the other methods, the EGM will not be extended to non-linear models. However, as mentioned before, the key point behind this process is to adopt a method that captures the history dependent behaviour of non-linear models, such as the stress update algorithm adopted for CEGM.

The EGM has a major advantage compared with FEMU and CEGM, it does not require the costly computations of a FE model. Consequently, it is less time consuming. Nevertheless, the implementation of this method is more laborious than in FEMU strategy. It also requires the availability of a strain field within the whole solid body (full-field measurements). Therefore, it is not so flexible as the FEMU and CEGM. In addition, the applied force distribution must be known, as for FEMU and CEGM, which can be difficult to obtain, unless the weak form of Eq. (21) is used.

3.4. Virtual fields method

The Virtual Fields Method (VFM) has received significant attention from the scientific community in the recent years. It was first introduced by Grédiac [14] and since then its effectiveness has been proved in a large range of applications. The complete theory of VFM and its applications can be found in [48]. The most recent applications, organized by

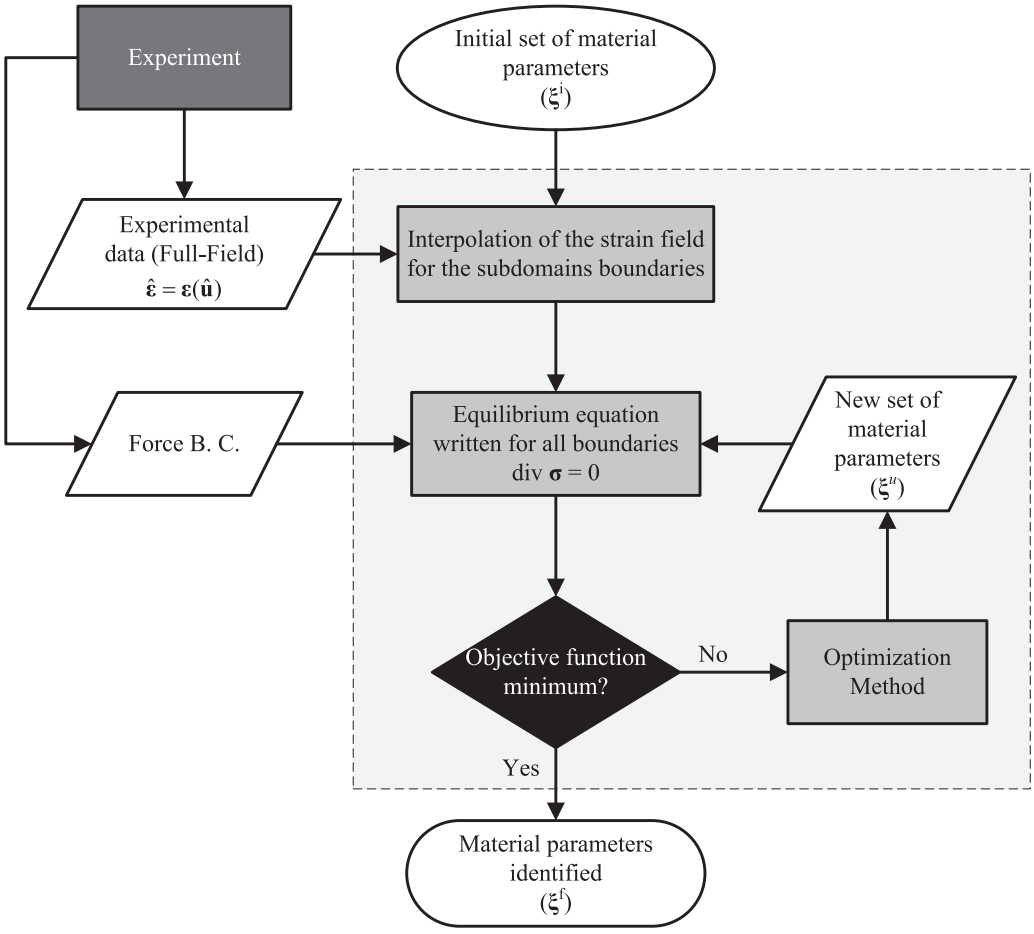

Fig. 5. Detailed flowchart for the EGM.

constitutive behaviours, are: anisotropic thermo-elasticity [49], hyper-elasticity [50], plasticity (anisotropic hardening, non-linear kinematic hardening and damage) [34,51,52], viscoplasticity [53] and temperature dependent viscoplasticity using isothermal tests [54].

The key elements behind VFM are the Principle of Virtual Work and a suitable choice of virtual fields. For the solid body shown in Fig. 1, in the absence of body-forces and assuming infinitesimal small displacements, the Principle of Virtual Work expresses that the internal virtual work must equal the external virtual work performed by the external forces and can be written as follows

$$\underbrace{\int_{\Omega} \boldsymbol{\sigma}(\boldsymbol{\xi}, \hat{\boldsymbol{\varepsilon}}) : \boldsymbol{\varepsilon}^{\star} dV}_{\text{Internalwork}} = \underbrace{\int_{\Gamma_f} \bar{\mathbf{f}} \cdot \mathbf{u}^{\star} dS}_{\text{Externalwork}}, \tag{23}$$

where $\boldsymbol{\varepsilon}^{\star}$ is a virtual strain field and $\mathbf{u}^{\star}$ is a virtual displacement field. dV and dS are the infinitesimal volume and area for the current domain of the solid body, respectively. The principle of virtual work is independent of any constitutive model, which, theoretically, allows to apply VFM to all types of constitutive models. Furthermore, the force distribution ($\bar{\mathbf{f}}$) is not required. Instead, the resultant of the applied force can be used with a suitable choice of virtual fields. Thus, the only unknown of the problem is the Cauchy stress tensor $\boldsymbol{\sigma}(\boldsymbol{\xi}, \hat{\boldsymbol{\varepsilon}})$, which depends on the set of material parameters. Considering elasticity case, the Cauchy stress tensor is computed using Eq. (3) and the measured displacement/strain field ($\hat{\boldsymbol{\varepsilon}} = \boldsymbol{\varepsilon}(\hat{\mathbf{u}})$). For this case, the material parameters can be evaluated directly from a system of equations. The system of equations has the same number of equations as number of unknown material parameters of the model.

For simplicity's sake, a different notation for the Eq. (3) is considered here [48,55]. Thus $\boldsymbol{\sigma}$ can be written in the matrix notation as

$$\begin{Bmatrix} \sigma_{xx} \\ \sigma_{yy} \\ \sigma_{xy} \end{Bmatrix} = \begin{bmatrix} Q_{xx} & Q_{xy} & 0 \\ Q_{yx} & Q_{yy} & 0 \\ 0 & 0 & Q_{ss} \end{bmatrix} \begin{Bmatrix} \hat{\varepsilon}_{xx} \\ \hat{\varepsilon}_{yy} \\ \hat{\varepsilon}_{xy} \end{Bmatrix}, \tag{24}$$

Replacing Eq. (24) in the principle of virtual work (Eq. (23)) and after some algebraic manipulation, it can be written

$$\begin{aligned} &Q_{xx} \int_{\Omega} \hat{\varepsilon}_{xx} \varepsilon^{\star}_{xx} dV + Q_{yy} \int_{\Omega} \hat{\varepsilon}_{yy} \varepsilon^{\star}_{yy} dV + Q_{xy} \int_{\Omega} \hat{\varepsilon}_{yy} \varepsilon^{\star}_{xx} dV \\ &\quad + Q_{yx} \int_{\Omega} \hat{\varepsilon}_{xx} \varepsilon^{\star}_{yy} dV + Q_{ss} \int_{\Omega} \hat{\varepsilon}_{xy} \varepsilon^{\star}_{xy} dV \\ &= \int_{\Gamma_f} \bar{f}_x \cdot u^{\star}_x dS + \int_{\Gamma_f} \bar{f}_y \cdot u^{\star}_y dS, \end{aligned} \tag{25}$$

where the variables Q_{xx}, Q_{yy}, Q_{xy}, Q_{yx}, Q_{ss} have been moved out of the integrals, since these are assumed as constants. In case of isotropic linear elasticity, the following relation exists between the terms: $Q_{yy} = Q_{xx}$, $Q_{yx} = Q_{xy}$ and $Q_{ss} = (Q_{xx} - Q_{xy})/2$. Accordingly, the Poisson's ratio and the Young's modulus can be expressed as $\nu = Q_{xx}/Q_{xy}$ and $E = Q_{xx}/(1 - \nu^2)$.

In order to retrieve the two unknown material parameters ($\boldsymbol{\xi} = \{\nu, E\}$), it is required two independent virtual fields. The number of virtual fields must be equal to the number of unknown material parameters and Eq. (25) must be written for each selected virtual field. The calculation of integrals in Eq. (25) can be approximated by discrete sums, as performed for the CEGM (Section 3.2). The result is a linear system of two equations with two unknowns, Q_{xx} and Q_{xy}, respectively.

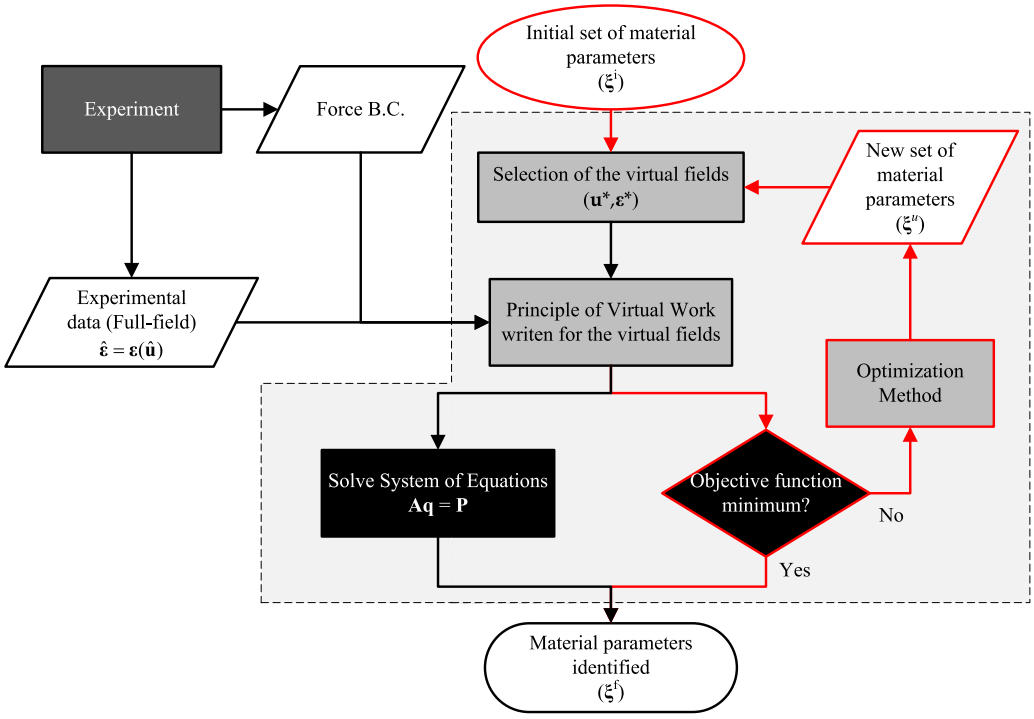

Fig. 6. Detailed flowchart for the VFM. Note that the red path is exclusive for non-linear constitutive models. (For interpretation of the references to colour in this figure legend, the reader is referred to the web version of this article.)

Provided that the measured strain field is heterogeneous and the chosen virtual fields are independent, the system of equations is linearly independent and can be written as

$$\mathbf{Aq} = \mathbf{P}, \tag{26}$$

where $\mathbf{A}$ is a square matrix composed by the strain terms, $\mathbf{q}$ is a vector of the unknown material coefficients $\{Q_{xx}, Q_{xy}\}$ and $\mathbf{P}$ is the vector of virtual external work of the applied forces. This linear system of equations is solved with a low computational cost.

For the case of a non-linear model, it is no longer possible to derive the linear system of equations and the identification process turns into an iterative procedure, which relies on the minimization of an objective function [48,56]. This objective function expresses the gap between the internal and the external virtual works and can be defined in a least square based formulation as

$$\mathcal{F}_{\mathrm{VFM}}(\boldsymbol{\xi}) = \sum_{i=1}^{n_s} \left(\int_{\Omega} \boldsymbol{\sigma}(\boldsymbol{\xi}, \hat{\boldsymbol{\varepsilon}}) : \boldsymbol{\varepsilon}^{\star} d\Omega - \int_{\Gamma_f} \bar{\mathbf{f}} \cdot \mathbf{u}^{\star} dS \right)_i^2, \tag{27}$$

The calculation of the stress field is performed through a stress update algorithm, as the one adopted for CEGM [44].

A detailed flowchart for VFM is presented in Fig. 6. Two different paths are represented. The first one (black lines) includes the main steps for the identification of material parameters of linear models. As mentioned above, for linear constitutive models the material parameters are retrieved after solving a system of linear equations (Eq. (26)). The second path (red lines) corresponds to non-linear constitutive models. In this case, the material parameters are retrieved after the cost function value reached a minimum or the process stagnation. The search for the minimum value is performed by means of an optimization method.

The choice of the virtual fields is part of the VFM identification process. An infinite number of virtual fields can be used, but a proper choice facilitates the identification process and can improve the quality of the final set of parameters. The suitable choice of the virtual fields has been pointed out as the major weakness of VFM, specially in non-linear cases [3,25]. It should be emphasized that, the virtual displacement and strain fields are just mathematical test functions and can be seen as weights [48,57]. Moreover, they can be defined independently of the measured displacement/strain strain field [48]. However, due to a matter of convenience, the virtual fields are usually defined in accordance with two conditions. First, the displacement boundary conditions must be satisfied, *i.e.*, at the boundary Γ_u the virtual displacement field must be zero ($\mathbf{u}^{\star} = \mathbf{0}$) [32,48]. The second condition is related to the use of the resultant of the applied force, instead of its distribution. Therefore, the virtual displacement fields must be chosen in order to be constant along the boundary Γ_f and, to eliminate the components of the resultant force that are unknown, $\mathbf{u}^{\star}$ must be collinear with $\bar{\mathbf{f}}$ [48,52]. Moreover, it is required that the virtual fields assure a C^0 continuity. Regarding the use of the applied force in VFM, in special cases such as dynamic testing, obtaining accurate measurements of the applied force can be difficult. A different formulation of Eq. (23), which includes the virtual work of the inertial forces, can then be used and the external virtual work term can be cancelled out using suitable virtual fields [48,58,59]. This approach has been exclusively applied to the identification of dynamic mechanical characteristics, thus it will not be addressed in this work.

A great effort has been made to suppress the major weakness of VFM and currently there are three strategies available for the choice of the virtual fields, which are:

(i) *Manually defined virtual fields*: This procedure is the most used in non-linear cases [34,51,57]. Usually, polynomials or sine/cosine functions are used [48]. This strategy is the easiest to implement, but it is user-dependent. Therefore, the search for a function that meet the conditions mentioned above depends on the expertise of the user. Moreover, there is no guarantee that the chosen virtual fields produce the best results.

(ii) *Stiffness-based virtual fields*: This second procedure has been a great step to overcome the previous drawbacks. It was first proposed by Avril et al. [60] for anisotropic elasticity and then extended to elasto-plasticity [56]. In this case, the calculation of the virtual fields requires the derivation of the tangent stiffness-matrix (in elasto-plasticity, the tangent elasto-plastic stiffness matrix (Eq. (14)). This strategy relies on a statistical approach to

quantify the uncertainty of the identified parameters due to noise on the measurements. Based on this, an automatic procedure to derive virtual fields that minimizes the effect of noise is designed. However, the implementation is a cumbersome task due to the calculation of the tangent elasto-plastic stiffness matrix.

(iii) *Sensitivity-based virtual fields*: Recently proposed by Marek et al. [57], this strategy offers an easier implementation procedure. In this case, the virtual fields are determined according to a sensitivity stress map, i.e., the virtual fields are determined to give more weight to the locations of the specimen where more information about a parameter is encoded [57]. Thus, the sensitivity of the stress field to each parameter must be tested to define a virtual field for each unknown material parameter.

The major advantage of VFM is that it does not need FE analysis. Therefore, when compared with strategies such as FEMU and CEGM, a superior computational efficiency is expected. Indeed, Zhang et al. [50] reported a significant drop on the time required to retrieve the material parameters. In their case, the VFM was 125 faster than the FEMU. Another important advantage of VFM is that it does not require the exact distribution of the applied force on the boundary Γ_f. With a proper choice of virtual fields, it only requires the force resultant in one direction, which is usually measured during experiments.

Like EGM, the main disadvantage of VFM is that it requires full-field experimental data over the entire domain, which is not as flexible as FEMU and CEGM. Moreover, in non-linear cases, like CEGM, VFM requires a tool for the calculation of the stress field from the measured strain field, often based on return-mapping algorithm.

4. Comparison of the different inverse strategies

The aim of this section is to compare the inverse strategies described in Section 3. Robustness in the presence of noisy data and computational efficiency are the two main aspects to be evaluated. Full-field measurements are generated with the aid of the FE method and a single numerical test with a heterogeneous strain field is used.

This section is presented in two parts. In the first part, the different strategies are evaluated in isotropic linear elasticity, for which Young's modulus and Poisson's ratio ($\boldsymbol{\xi} = \{E, \upsilon\}$) are the unknown material parameters. In the second part, the different strategies are evaluated in isotropic elasto-plasticity for the model presented in Section 2, and the set of parameters $\boldsymbol{\xi} = \{K, \varepsilon_0, n\}$ is identified. For this last part, the elastic parameters are considered to be known *a priori*.

The analysis was carried out with a standard computer, with an Intel(R) Core(TM) i7-4770 (3.40 GHz) processor and 8.00 GB of RAM memory. The computational time presented for each strategy is the *wall-time* or *real-time clock*, which means the total time of a task including input/output activities.

4.1. Heterogeneous test

In order to easily and clearly compare the different strategies, a numerical test is designed to be simple, but also to generate a heterogeneous strain field. It consists of a solid with dimensions 3×3 mm^2 in-plane and thickness of $t = 0.1$ mm. The solid is discretized with 4-node bilinear elements, making a total of 9 plane-stress elements and 16 nodes. Fig. 7 (a) presents the initial geometry and the boundary conditions, as well as the finite element mesh. x and y are the local coordinates along the horizontal and vertical axes, according to the reference system. The boundaries $x = 0$ and $y = 0$ are fixed and the force boundary condition is applied on the boundary $x = 3$ mm. The force boundary condition has a non-uniform distribution along the $y-$coordinate and a single component in the $x-$direction. The distribution of this load changes linearly with y, as: $f_x(y) = my + b$. The variables m and b control the distribution. Although tension is the main stress state corresponding to this load, the other components of the stress tensor are also active.

Table 1
Identification results in elasticity.

	E [GPa]	ν	Iterations	Normalized wall-time
Reference parameters	210.00	0.3000		
FEMU	210.00	0.3000	10	1.000
CEGM	210.00	0.2993	12	0.444
EGM	210.97	0.2874	9	0.167
VFM	210.00	0.3000	(–)	(–)

Regarding the identification process, the force distribution is assumed to be known. This is useful to build up the FE model for FEMU and CEGM, and also for the EGM, since to establish the local equilibrium at the boundary Γ_f, Eq. (21) must be determined. In contrast, VFM does not require the force distribution, which is an important aspect to alleviate constraints in the design of a mechanical test.

4.2. Identification of material parameters using full-field measurements in linear elasticity

In this part, the reference material assumed for the model of Fig. 7 (a) is considered homogeneous and isotropic linear elastic. The reference material parameters, Poisson's ratio and Young's modulus, are $\nu = 0.3$ and $E = 210.00$ GPa, respectively. The distribution of the force boundary condition is defined by $m = 10$ Nmm^{-1} and $b = 50$ N. The numerical results are generated using an in-house FE code dedicated to linear elastic problems. The distribution of the components of the infinitesimal strain tensor are shown in Fig. 7 (b), (c) and (d). It can be seen that the test is heterogeneous, which results from the non-uniform distribution of the applied force. The strain tensor, used in the different strategies, is derived from the displacement field using the derivatives of the FE shape functions. It is calculated at the integration points and output at the nodes. This leads to an information at 16 points, instead of 9 if the centroid of the elements was used.

To perform the identification using FEMU, CEGM and EGM, an initial set of material parameters is required, so the following set was defined: $\boldsymbol{\xi} = \{E, \upsilon\} = \{0.2, 100.00 \text{ GPa}\}$. Regarding the determination of a statically admissible stress field for CEGM, the same initial set of material parameters is used. This stress field is not updated during the process, since the material properties are homogeneous over the body. A gradient-based optimization algorithm, called Generalized Reduced Gradient (GRG) [61], is chosen. The threshold value for the cost function and for the variation of each parameter between iteration is set to 1×10^{-8}.

In contrast to the former strategies, VFM does not require an optimization method, but requires a suitable choice of virtual fields. Following the manual approach (see Section 3.4), two different virtual fields are chosen, which can be written as

$$\mathbf{u}^{\star(1)} = \begin{Bmatrix} u_x^{\star(1)} = x \\ u_y^{\star(1)} = 0 \end{Bmatrix} \Rightarrow \quad \boldsymbol{\varepsilon}^{\star(1)} = \begin{Bmatrix} \varepsilon_{xx}^{\star(1)} = 1 \\ \varepsilon_{yy}^{\star(1)} = 0 \\ \varepsilon_{xy}^{\star(1)} = 0 \end{Bmatrix}, \tag{28}$$

$$\mathbf{u}^{\star(2)} = \begin{Bmatrix} u_x^{\star(2)} = 0 \\ u_y^{\star(2)} = y \end{Bmatrix} \Rightarrow \quad \boldsymbol{\varepsilon}^{\star(2)} = \begin{Bmatrix} \varepsilon_{xx}^{\star(2)} = 0 \\ \varepsilon_{yy}^{\star(2)} = 1 \\ \varepsilon_{xy}^{\star(2)} = 0 \end{Bmatrix}. \tag{29}$$

The selected virtual fields have the simplest possible form. Both virtual fields satisfy the displacement boundary conditions and the first one reduces the use of the applied force to its resultant along the $x-$direction. It is also noteworthy that, with the selected virtual fields, the same weight is given to each measurement point ($\varepsilon_{xx}^{\star(1)} = 1$ and $\varepsilon_{yy}^{\star(2)} = 1$).

The results of the identification process for each strategy are presented in Table 1. FEMU, CEGM and VFM accurately retrieve the material parameters. EGM leads to good results for Young's modulus, but the deviation for Poisson's ratio is around 4% . This small error can be

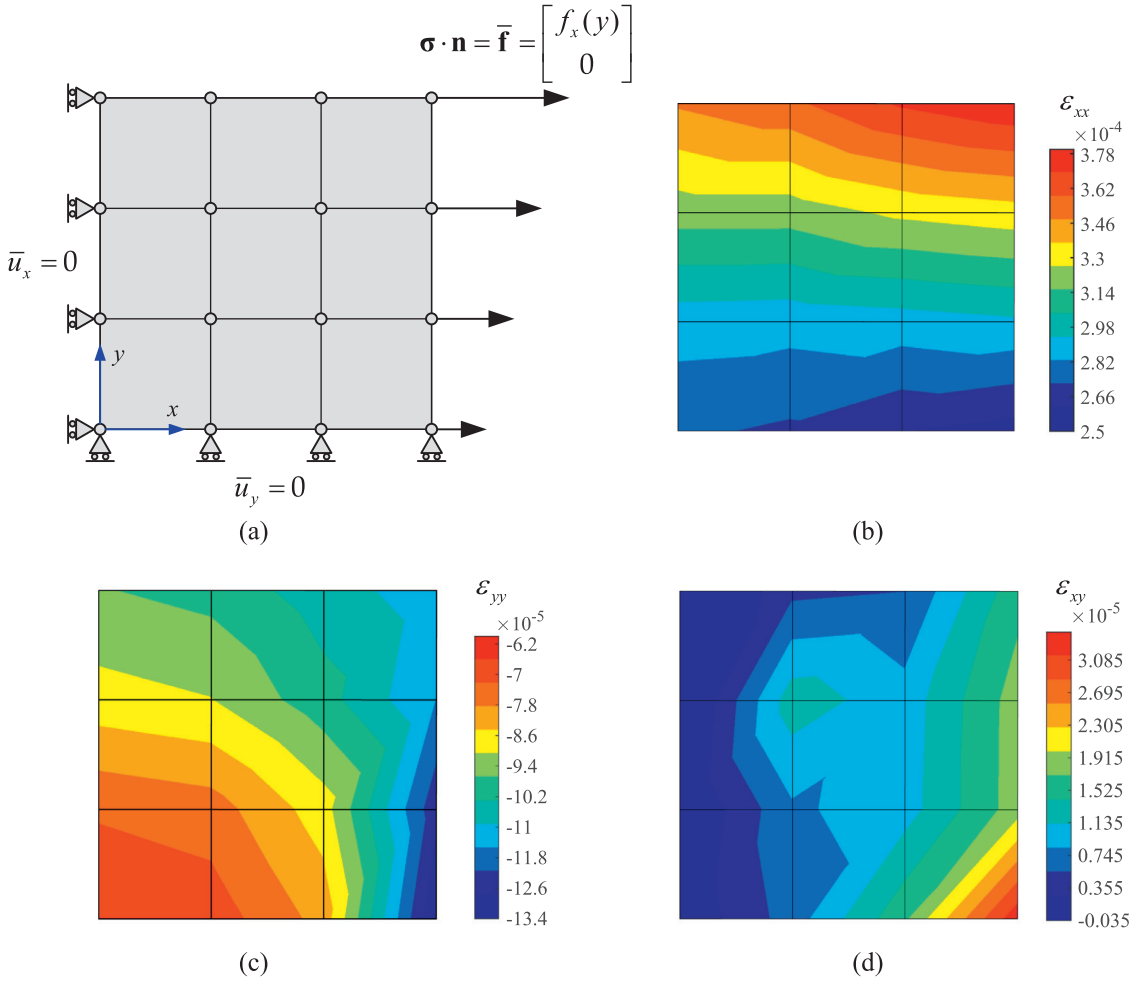

Fig. 7. Heterogeneous test: (a) initial geometry, mesh and boundary conditions of the test; and components of the infinitesimal strain tensor; (b) ε_{xx}, (c) ε_{yy} and (d) ε_{xy}.

attributed to the interpolation process. According to the presented results, it is possible to conclude that the four strategies were implemented correctly.

The number of iterations for each method is also evaluated and is presented in Table 1. CEGM requires a larger number of iterations than the other strategies. However, when compared with FEMU, CEGM requires a single FE simulation to determine the admissible stress field, whereas FEMU needs a FE simulation at each evaluation of the cost function. This is reflected in the normalized wall-time, also presented in Table 1. The wall-time of the FEMU strategy is used for normalization, since it has the highest value. The normalization is adopted here because the values are too low. In terms of the iterative strategies (FEMU, CEGM and EGM), EGM presents the lowest value for the wall-time. The wall-time for VFM is close to zero, indeed, it just requires time for the inversion of a 2×2 matrix and its multiplication by the vector of virtual external work (Eq. (26)), which are simple operations.

Experimental measurements acquired by DIC are inevitably affected by errors from different sources, such as out-of-plane movements, quality of the speckle, interpolation errors and so on. These errors have an important effect on the measured displacement field and then on the computed strain field. This affects the quality of the identified material parameters. Therefore, testing the robustness and stability of the identification strategies when fed with data corrupted with errors is an important aspect. To this purpose, Rossi et al. [62] proposed a simulator able to numerically reproduce the entire chain of acquisition of experimental measurements with DIC, which can be used to identify

Table 2
Identification results in elasticity with noisy data (error magnitude of 1×10^{-6}).

	E [GPa]	ν	E - Error[%]	ν - Error[%]
Reference parameters	210.00	0.3000		
FEMU	203.90	0.2706	2.90	9.798
CEGM	204.55	0.2728	2.59	9.058
EGM	195.10	0.2356	7.09	21.436
VFM	205.14	0.2753	2.31	8.207

the effect of this errors in the identification process. Here, a simple approach, though enough to evaluate the performance of the identification strategies in the presence of errors, is adopted, which consists in adding a random error to the computed strain field. The random error with a zero-mean Gaussian distribution and standard deviation of 1 is added to the reference strain field used above. The magnitude of the error is of the order 1×10^{-6}. The results with noisy data are presented in Table 2. It is also presented the relative error for each parameter, which is calculated relatively to the reference values. The CPU normalized times for each strategy are similar to the one presented in Table 1.

Table 2 shows that EGM presents the highest level of error for both parameters, with almost 21% of error for Poisson's ratio and 7% for Young's modulus. EGM has the highest sensitivity to noise in this case. The other three strategies give similar results, with an error lower than 3% for Young's Modulus and lower than 10% for Poisson's ration. Nev-

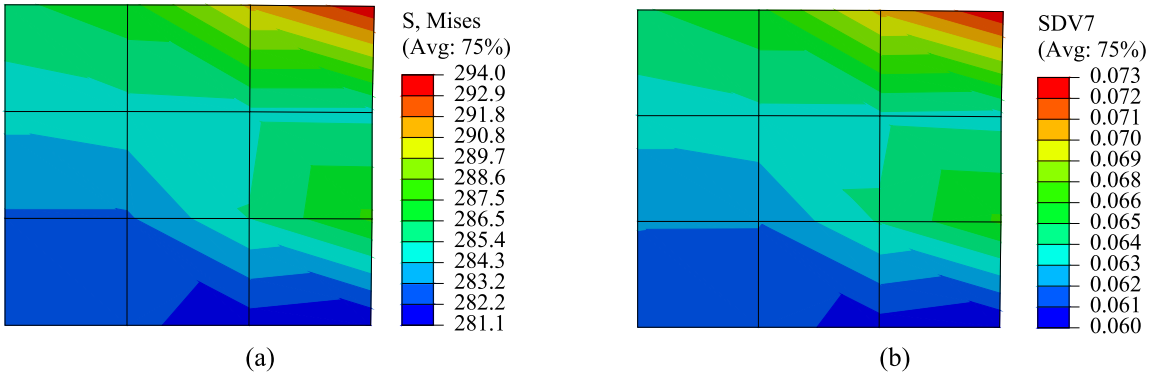

Fig. 8. (a) von Mises stress distribution and (b) equivalent plastic strain field at the end of the test.

ertheless, VFM presents the lowest level of error for both parameters, followed by CEGM and finally, FEMU. In conclusion, for this specific case, VFM is the most robust strategy in the presence of noisy data and EGM is the least robust.

Although not addressed in this study, it should be mentioned that the results obtained for noisy data with VFM, according to [48], could be improved through the use of stiffness-based virtual fields, which are specially designed to minimize the effect of noise (see Section 3.4).

4.3. Identification of material parameters using full-field measurements in elasto-plasticity

In this second part, it is addressed the identification of the material parameters for non-linear models, namely the isotropic elasto-plastic model presented in Section 2. The material parameters for the elastic part are the same of the last section ($E = 210$ GPa and $\nu = 0.3$) and it is assumed that they are known *a priori*. Thus, the material parameters to be identified are the parameters of the Swift's Law (Eq. (8)), for which the following reference values are adopted: $\boldsymbol{\xi} = \{K, \varepsilon_0, n\} = \{565\ \text{MPa}, 7.81 \times 10^{-3}, 0.26\}$. The numerical results are generated using the FE code ABAQUS standard. The numerical model is built up using an element CPS4 (bilinear shape functions and full integration) along with the mesh of Fig. 7 (a). A small displacement formulation is also adopted. Regarding the force boundary condition applied to the model, the following parameters are adopted: $m = 10\ \text{Nmm}^{-1}$ and $b = 270$ N.

The input data for all the methods is still the strain field, but the strain tensor is output at the centroid of the elements. Therefore, only 9 points are available. The force resultant is extracted on the boundary Γ_f.

The FE analysis is discretized in five equal increments, with a constant increment size of 0.2. As a result, five strain fields are available for the identification. For the first two increments, the body undergoes only elastic deformations and the yielding process starts in the third increment. The distributions of the von Mises stress and the equivalent plastic strain field at the end of the test are shown in Fig. 8.

Due to the non-linearity of the model, VFM assumes the form of the objective function presented in Section 3.4. Nevertheless, it requires the selection of a virtual field to write the principle of virtual work. Only one virtual field is chosen in order to keep the process as simple as possible. Hence, the first virtual field presented in Eq. (28) ($\mathbf{u}^{\star(1)}$) is adopted.

The objective functions of the different methods (FEMU, CEGM and VFM) are minimized with the Levenberg–Marquardt optimization method [63]. This is a least-square gradient-based optimization method which requires the derivative of the objective functions. Forward differences are adopted for the calculation of the derivatives. The convergence criterion is similar to the one used in Section 4.2, but with a value of 1×10^{-5}. Generally, constraints on the domain of the material parameters are assigned *a priori*. However, in this work, this will be avoided, unless required for a strategy to achieve a solution.

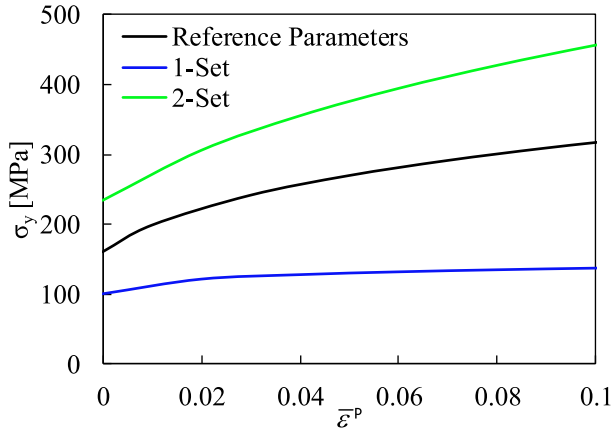

Fig. 9. Flow stress evolution according to the Swift's law for the initial sets of material parameters listed in Table 3.

Table 3
Initial sets of material parameters for the Swift's law (1-Set and 2-Set) used to start the identification process.

Parameters	K [MPa]	ε_0	n
Reference	565	7.81×10^{-3}	0.26
1-Set	165	2.00×10^{-3}	0.08
2-Set	965	1.76×10^{-2}	0.35

CEGM and VFM require the reconstruction of the stress field from the numerically generated strain field. For both strategies, it is adopted an implicit backward-Euler stress update algorithm presented in [44].

Such an identification is a more difficult process than the previously performed one, mainly due to the non-linear nature of the model, the coupling between the parameters and also the number of parameters. The presence of local minima in the objective function is one of the aspects that can stop the process and lead to erroneous solutions. Therefore, in order to evaluate the robustness of the presented strategies, two different initial sets of material parameters are arbitrarily selected. The two sets are presented in Table 3 and the respective flow stress curves given by Swift's law are presented in Fig. 9.

The results of the identification process for the different strategies are summarized in Table 4. CEGM and VFM correctly retrieve the three parameters, independently of the initial set of parameters. This indicates that the reference solution is a global minimum within the interval delimited by the selected initial sets (see Table 3). Figs. 10 and 11 present the evolution of the material parameters along the identification process, as well as the evolution of the value of the objective functions,

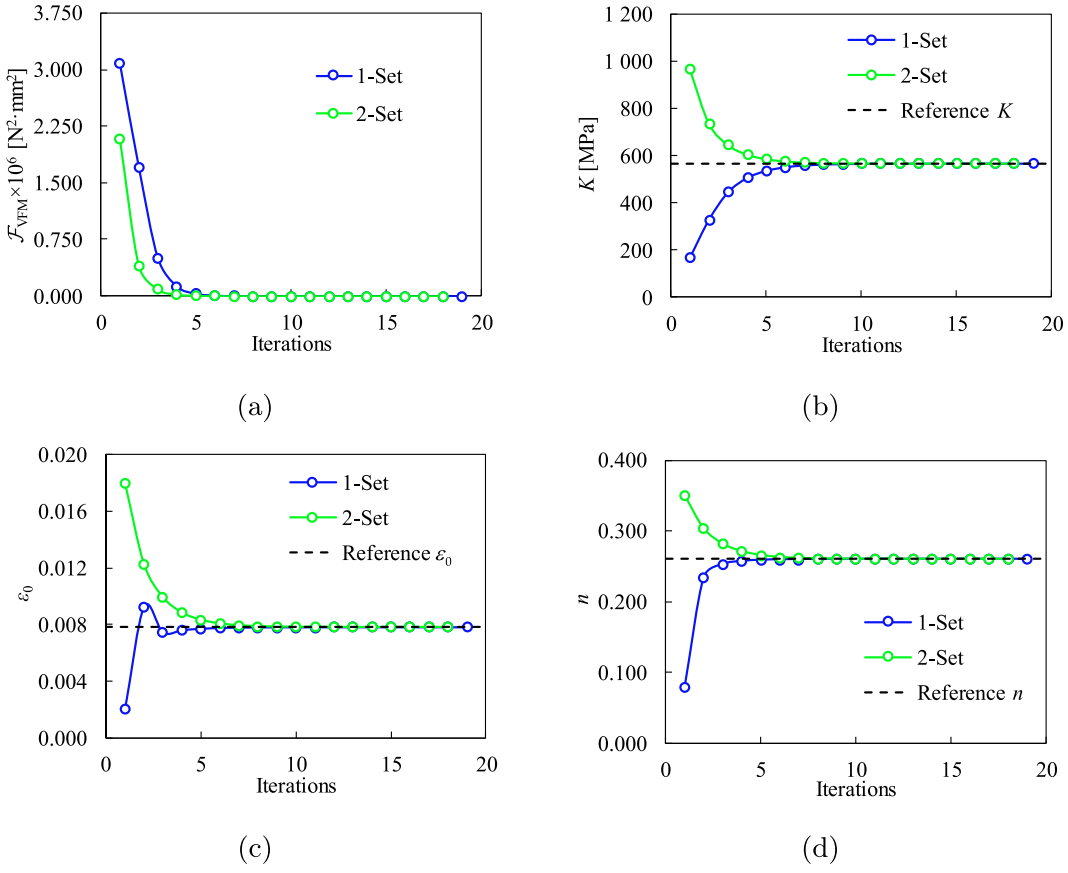

Fig. 10. Results of the identification process for VFM strategy: (a) objective function evolution; parameters (b) K; (c) ε_0 and (d) n evolutions.

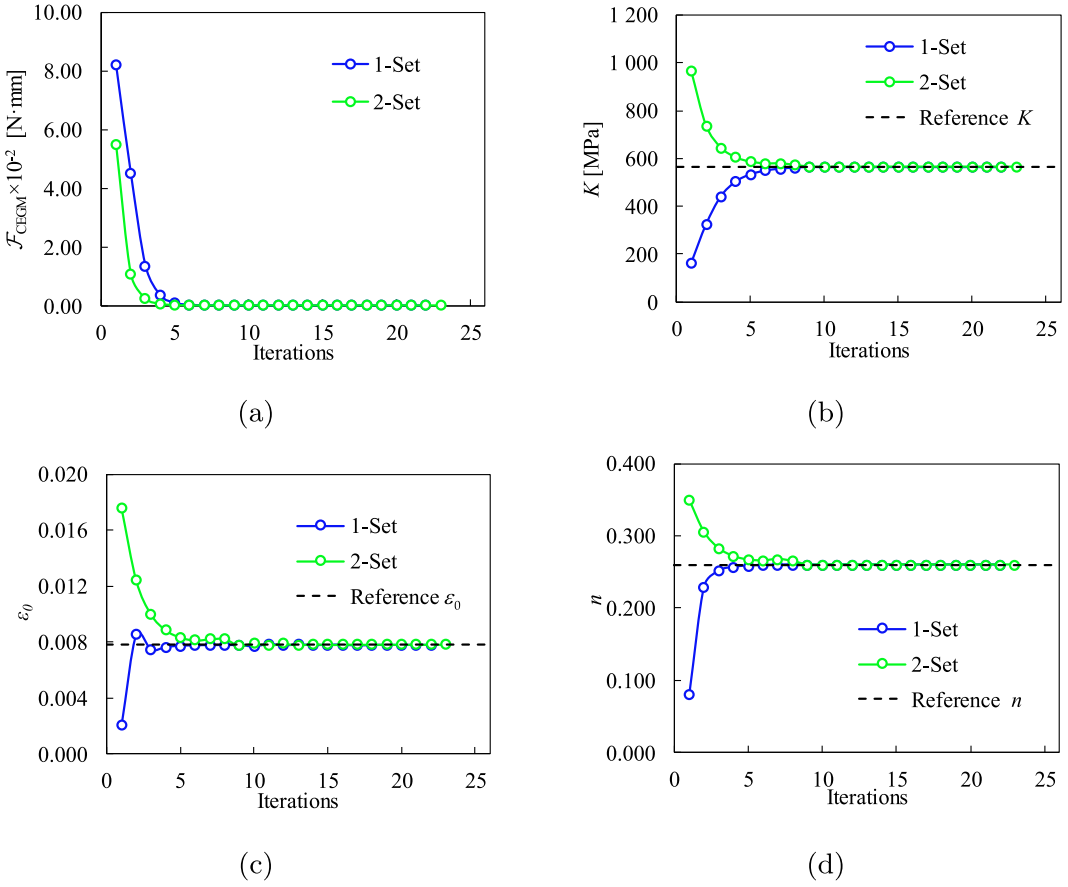

Fig. 11. Results of the identification process for CEGM strategy: (a) objective function evolution; parameters (b) K; (c) ε_0 and (d) n evolutions.

Table 4
Identification results in elasto-plasticity (isotropic hardening described by Swift's law).
*Constraint on the material parameters domain.

	Parameters	K [MPa]	ε_0	n	Iterations	Wall-time [s]
	Reference	565	7.810×10^{-3}	0.260		
FEMU	1-Set*	564.998	7.809×10^{-3}	0.259	41	4407.5
	2-Set	565.000	7.808×10^{-3}	0.260	20	2048.9
CEGM	1-Set	564.317	7.761×10^{-3}	0.259	22	38.5
	2-Set	564.985	7.819×10^{-3}	0.260	23	36.9
VFM	1-Set	565.080	7.795×10^{-3}	0.260	19	10.3
	2-Set	565.085	7.795×10^{-3}	0.260	18	7.8

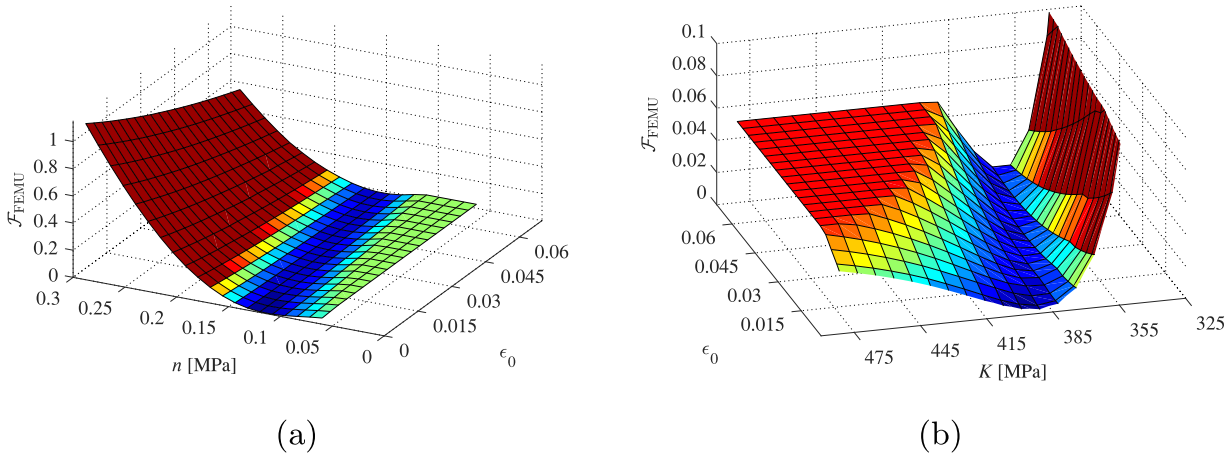

Fig. 12. Plots of the objective function of FEMU for: (a) $K = 386.691$ MPa; (b) $n = 0.113$.

for both strategies. These figures reveal that both strategies have fast convergence.

FEMU strategy is able to retrieve the material parameters when the identification starts from the 2-Set of initial parameters. However, for the 1-Set, the presence of a local minimum in the cost function for the values of the parameters $K = 386.691$ MPa and $n = 0.113$ leads to negative values of the parameter ε_0, which is not admissible for Swift's law. The presence of this local minimum can be seen in Fig. 12. Therefore, in order to guarantee positive values for the solution parameters, a constraint on the material parameters domain must be added and kept through the remaining part of this study. Besides, the convergence of FEMU is not so fast as in the case of CEGM and VFM, as can be observed in Fig. 13.

The iterations and wall-time are also presented in Table 4. VFM provides the lowest wall-time, with an average of 0.48 s per iteration. CEGM is more than 3 times slower than VFM and has an average of 1.7 s per iteration. FEMU presents the worst results for the wall-time. For the 1-Set, VFM is almost 428 times faster than FEMU and for the 2-Set, VFM is 263 times faster than FEMU, which are significant differences. The choice of the initial set of parameters strongly affects the wall-time in the case of FEMU, a consequence of the required number of iterations. The identification which starts from 1-Set is clearly hampered by the presence of local minima, which led to an increase of the iterations number and, consequently, to the increase of the wall-time.

As performed for the elastic case, the effect of noise on the identification process is also addressed in this case and the sensitivity of the different strategies is evaluated. A random error with a zero-mean Gaussian distribution and standard deviation of 1 is added to the reference strain fields used in the previous results. Two levels of noise are tested, the first one with a magnitude of order 1×10^{-5} and the other with a magnitude of order 1×10^{-4}. The results for each noise level are presented in Tables 5 and 6.

For the first level of noise (magnitude of order 1×10^{-5}, Table 5), the three strategies retrieve the material parameters with a good accuracy, independently of the initial set of parameters. This indicates that the reference set of parameters gives a global minimum. Nevertheless, VFM has a slight deviation on the parameter ε_0, but the error is below 1.4%.

For the second level of error (magnitude of order 1×10^{-4}, Table 6), FEMU correctly retrieves the material parameters, with errors below 0.5%. The initial set has no influence on the accuracy of the results. CEGM underestimates the values of the three parameters for both initial sets and has the highest error for the parameter ε_0, with an error around 97%. VFM has reasonable results for the parameters K and n, with errors below 4%. Nevertheless, it overestimates the parameter ε_0.

The parameter ε_0 dictates the beginning of the plastic regime, i.e., it defines the initial yield stress ($\sigma_0 = K\varepsilon_0^n$). As the number of time steps used is reduced and these do not capture the exact instant of transition between elastic and plastic regime, it can be difficult to retrieve this parameter. Nevertheless, using the results obtained with VFM to calculate the initial yield stress, the following values are obtained: 162.71 MPa and 162.84 MPa for the 1-Set and 2-Set, respectively. Comparing these with the reference value, which is 160 MPa, gives an error around 0.02%, which is admissible. It is also possible to see in Fig. 14 that the identified material parameters capture the correct evolution of the reference yield stress curve. In the case of CEGM, the obtained values for the initial yield stress are: 105.98 MPa and 107.87 MPa for the 1-Set and 2-Set, respectively. The errors for these two values are around 33%, which continues to be a significant difference. Moreover, the solutions obtained are also plotted in Fig. 14. It is possible to see the difference for the reference solution in the initial yield stress, but for higher values of equivalent plastic strain, the evolution of Swift's law is close to the reference one. For the case of FEMU the results are in good agreement with the reference, which is also highlighted in Fig. 14.

In Tables 5 and 6 is also presented the objective function value for the obtained solutions. Comparing the values of Table 5 with their counterparts in Table 6, an increase in the objective function value and parameters deviation with increasing values of noise can be observed. This is expected because the strain fields used as input data are no longer ex-

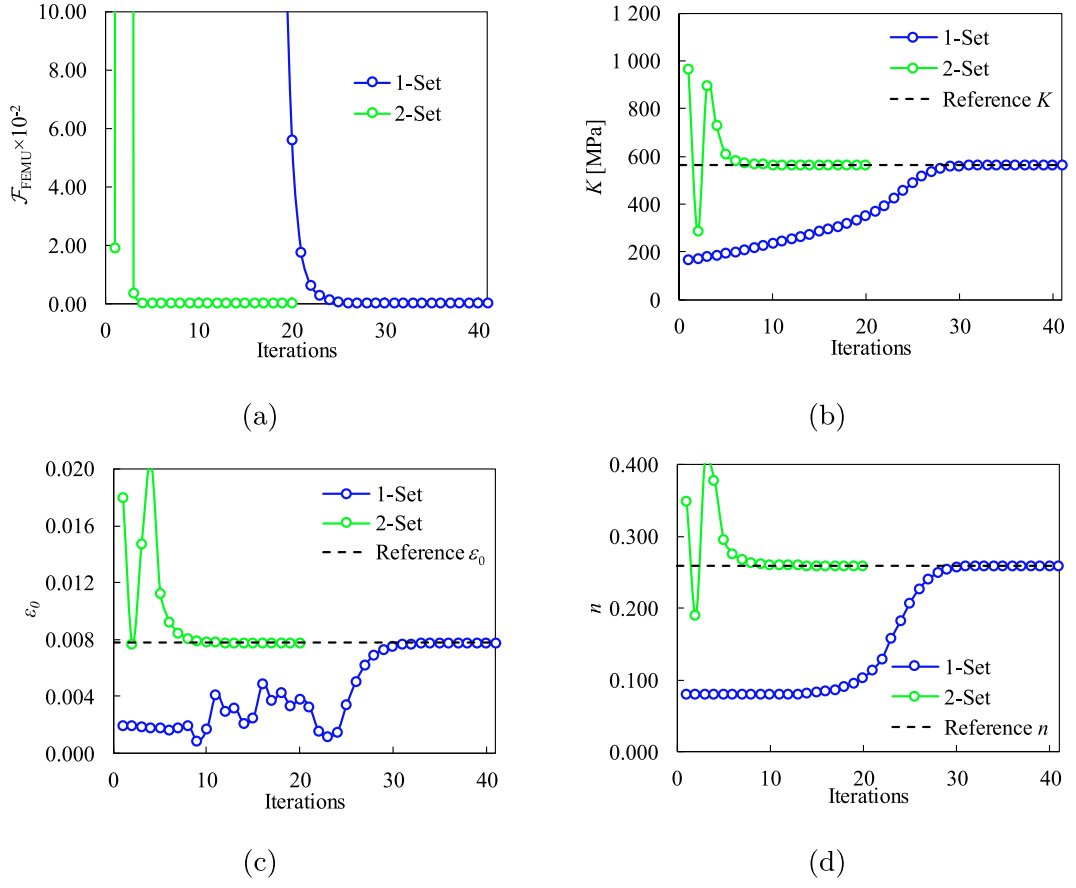

Fig. 13. Results of the identification process for FEMU strategy: (a) objective function evolution; parameters (b) K; (c) ε_0 and (d) n evolutions.

Table 5
Identification results in elasto-plasticity (isotropic hardening described by Swift's law) with noisy data (magnitude of order 1×10^{-5}). *Constraint on the material parameters domain.

		Parameters	K [MPa]	ε_0	n	Iterations	Obj. Func.
		Reference	565	7.810×10^{-3}	0.260		
FEMU		1-Set*	564.912	7.806×10^{-3}	0.259	42	1.29×10^{-8}
	Error		0.016%	0.051%	0.385%		
		2-Set	564.912	7.806×10^{-3}	0.259	18	1.29×10^{-8}
	Error		0.016%	0.051%	0.385%		
CEGM		1-Set	565.421	7.852×10^{-3}	0.260	34	4.36×10^{-5} N · mm
	Error		0.074%	0.537%	0.156%		
		2-Set	566.536	7.904×10^{-3}	0.261	20	4.36×10^{-5} N · mm
	Error		0.272%	1.203%	0.425%		
VFM		1-Set	566.135	7.915×10^{-3}	0.261	15	17.9 $N^2\cdot mm^2$
	Error		0.201%	1.344%	0.363%		
		2-Set	566.186	7.916×10^{-3}	0.261	13	17.9 $N^2\cdot mm^2$
	Error		0.209%	1.357%	0.367%		

act solutions of the direct problem and move away from this solution with the noise increase. The question that arises here is, for noisy data, whether the reference set remains a minimizer of the objective functions and whether the solutions obtained are only local minima. The results in Table 5 indicate that the reference set remains the global minimizer for the noise magnitude of 1×10^{-5}, since the reference set has been retrieved by the three strategies with small values of error, independently of the initial set of parameters. However, for Table 6, the results of CEGM and VFM have a higher error, particularly for CEGM. Therefore, in order to understand whether the reference solution remains a minimizer for this level of noise, the objective functions have been evaluated for the reference set and the values are: $\mathcal{F}_{FEMU}=1.284\times10^{-6}$, $\mathcal{F}_{CEGM}=3.243\times10^{-3}$ N · mm and $\mathcal{F}_{VFM}=2031.2$ $N^2\cdot mm^2$. The result for the objective function of FEMU is close to the ones presented in Table 6, which supports that for FEMU the reference set remains a minimizer for this level of error. For the other two strategies, these values of the objective functions are higher than the final values presented in Table 6, indicating that the reference set of material parameters is no longer the global minimizer in both strategies and the obtained results are the new ones. It means that higher values of noise can modify the objective functions of CEGM and VFM, thus preventing the correct parameters from being retrieved. As mentioned at the end of Section 4.2, the results of VFM could be improved if stiffness-based or sensitivity-based virtual fields had been used [57].

In conclusion, it seems that FEMU exhibits the lowest sensitivity to the presence of noisy data, in this example. The CEGM revealed the highest sensitivity to noise. The higher sensitivity to noise presented by CEGM and VFM when compared with FEMU, can be explained by

Table 6
Identification results in elasto-plasticity (isotropic hardening described by Swift's law) with noisy data (magnitude of order 1×10^{-4}). *Constraint on the material parameters domain.

		Parameters	K [MPa]	ε_0	n	Iterations	Obj. Func.
		Reference	565	7.810×10^{-3}	0.260		
FEMU		1-Set*	564.128	7.783×10^{-3}	0.259	38	1.29×10^{-6}
	Error		0.154%	0.345%	0.385%		
		2-Set	564.127	7.783×10^{-3}	0.259	16	1.29×10^{-6}
	Error		0.154%	0.345%	0.385%		
CEGM		1-Set	441.906	1.838×10^{-4}	0.166	62	2.96×10^{-3} N · mm
	Error		21.787%	97.646%	36.309%		
		2-Set	464.445	2.617×10^{-4}	0.177	143	3.08×10^{-3} N · mm
	Error		17.797%	96.649%	31.954%		
VFM		1-Set	576.854	9.203×10^{-3}	0.269	11	1796.1 $N^2 \cdot mm^2$
	Error		2.098%	17.839%	3.826%		
		2-Set	577.413	9.212×10^{-3}	0.270	10	1795.1 $N^2 \cdot mm^2$
	Error		2.197%	17.951%	3.866%		

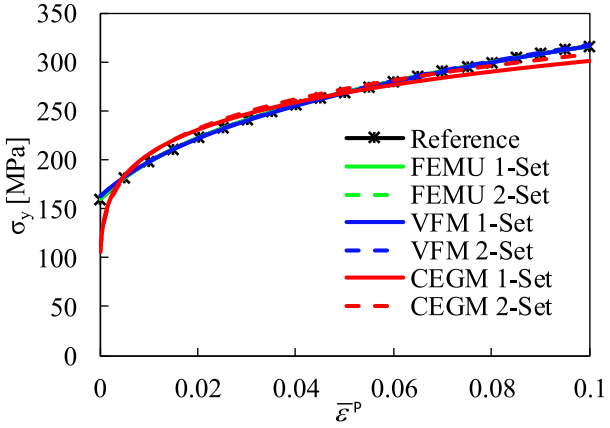

Fig. 14. Flow stress evolution according to Swift's law, for the identified sets of material parameters listed in Table 6.

the fact that, with FEMU the strain field is used directly to build up the objective function, whereas with CEGM and VFM, it is required the computation of the stress field that may lead to an amplification of the noise effect.

In terms of computational efficiency, the VFM has reached the best results with a significant margin for the other strategies, particularly for FEMU.

5. Conclusions

The calibration of constitutive models performed with full-field measurements is an increasingly used approach. Over the years, several strategies have been reported with successful results for linear and non-linear models. Therefore, it is important to understand and realize the advantages and drawbacks of each strategy, as well as their implementation aspects. This work is focused on four identification strategies based on full-field measurements, namely the Finite Element Model Updating (FEMU), the Constitutive Equation Gap Method (CEGM), the Equilibrium Gap Method (EGM) and the Virtual Fields Method (VFM). A brief overview of these strategies is presented, including their flowcharts and implementation details.

A comparative study is then performed. Two types of constitutive models are used: an isotropic linear elastic model and an elasto-plastic model with isotropic hardening described by Swift's law. In order to identify the material parameters of these two models, a FE model with a simple geometry is designed. The heterogeneous response of the FE model is generated by applying a non-uniform load distribution. The strain fields resultant from the solution of the direct problem are used as input for the different strategies. Hence, the four strategies are compared in the same conditions. Moreover, for both models, the robustness of the different strategies is tested against noisy data.

The results show an accurate performance of the different methods in elasticity, with the exception of EGM, which reveals a higher sensitivity to noise than the other methods. For the case of elasto-plasticity, FEMU achieves the most accurate results in the presence of data polluted with noise. Nevertheless, the computational time is significantly higher for FEMU. Moreover, in this specific case, it requires the use of constrains on the parameters domain to obtain admissible solutions. CEGM shows the highest sensitivity to noise, but in terms of computational cost, it is more efficient than FEMU. VFM has reasonable results in the presence of noise, and the best results for the computational cost. Moreover, improvements on VFM concerning noise sensitivity have already been performed and the results presented in this article could be further improved through the use of more advanced virtual fields. Therefore, VFM can be a perfect candidate when is expected a reasonable balance between quality of the identification procedure and computational cost.

Acknowledgements

The authors gratefully acknowledge the financial support of the Portuguese Foundation for Science and Technology (FCT) under the project P2020-PTDC/EMS-TEC/6400/2014 (POCI-01-0145-FEDER-016876) by UE/FEDER through the program COMPETE 2020 and UID/EMS/00481/2013-FCT under CENTRO-01-0145-FEDER-022083. The authors also would like to acknowledge the Région Bretagne (France) for its financial support. J.M.P. Martins is also grateful to the FCT for the PhD grant SFRH/BD/117432/2016.

References

[1] Barlat F, Brem J, Yoon J, Chung K, Dick R, Lege D, et al. Plane stress yield function for aluminum alloy sheets-part 1: theory. Int J Plast 2003;19(9):1297–319. doi:10.1016/S0749-6419(02)00019-0.
[2] Bruschi S, Altan T, Banabic D, Bariani P, Brosius A, Cao J, et al. Testing and modelling of material behaviour and formability in sheet metal forming. CIRP Ann 2014;63(2):727–49. doi:10.1016/j.cirp.2014.05.005.
[3] Prates P, Pereira A, Sakharova N, Oliveira M, Fernandes J. Inverse strategies for identifying the parameters of constitutive laws of metal sheets. Adv Mater Sci Eng 2016;2016:1–18. doi:10.1155/2016/4152963.
[4] Markiewicz E, Langrand B, Notta-Cuvier D. A review of characterisation and parameters identification of materials constitutive and damage models: from normalised direct approach to most advanced inverse problem resolution. Int J Impact Eng 2017;110:371–81. doi:10.1016/j.ijimpeng.2017.01.028.
[5] Sutton MA. Computer vision-based, noncontacting deformation measurements in mechanics: a generational transformation. Appl Mech Rev 2013;65(5):050802–050802–23. doi:10.1115/1.4024984.
[6] Zhang S, Leotoing L, Guines D, Thuillier S. Potential of the cross biaxial test for anisotropy characterization based on heterogeneous strain field. Exp Mech 2015;55(5):817–35. doi:10.1007/s11340-014-9983-y.
[7] Grédiac M, Hild F. Full-field measurements and identification in solid mechanics. John Wiley & Sons; 2012.

[8] Bonnet M, Constantinescu A. Inverse problems in elasticity. Inverse Probl 2005;21(2):R1.

[9] Avril S, Pierron F, Pannier Y, Rotinat R. Stress reconstruction and constitutive parameter identification in plane-stress elasto-plastic problems using surface measurements of deformation fields. Exp Mech 2008;48(4):403–19. doi:10.1007/s11340-007-9084-2.

[10] Kavanagh KT, Clough RW. Finite element applications in the characterization of elastic solids. Int J Solids Struct 1971;7(1):11–23. doi:10.1016/0020-7683(71)90015-1.

[11] Ladeveze P, Leguillon D. Error estimate procedure in the finite element method and applications. SIAM J Numer Anal 1983;20(3):485–509. doi:10.1137/0720033.

[12] Claire D, Hild F, Roux S. Identification of damage fields using kinematic measurements. Compt Rendus Mécanique 2002;330(11):729–34. doi:10.1016/S1631-0721(02)01524-3.

[13] Claire D, Hild F, Roux S. A finite element formulation to identify damage fields: the equilibrium gap method. Int J Numer Methods Eng 2004;61(2):189–208. doi:10.1002/nme.1057.

[14] Grédiac M. Principe des travaux virtuels et identification. Comptes rendus de l'Académie des sciences Série 2, Mécanique, Physique, Chimie, Sciences de l'univers, Sciences de la Terre 1989;309(1):1–5.

[15] Moussawi A, Lubineau G, Florentin E, Blaysat B. The constitutive compatibility method for identification of material parameters based on full-field measurements. Comput Methods Appl Mech Eng 2013;265:1–14. doi:10.1016/j.cma.2013.06.003.

[16] Blaysat B, Florentin E, Lubineau G, Moussawi A. A dissipation gap method for full-field measurement-based identification of elasto-plastic material parameters. Int J Numer Methods Eng 2012;91(7):685–704. doi:10.1002/nme.4287.

[17] Yun GJ, Shang S. A self-optimizing inverse analysis method for estimation of cyclic elasto-plasticity model parameters. Int J Plast 2011;27(4):576–95. doi:10.1016/j.ijplas.2010.08.003.

[18] Réthoré J. A fully integrated noise robust strategy for the identification of constitutive laws from digital images. Int J Numer Methods Eng 2010;84(6):631–60. doi:10.1002/nme.2908.

[19] Rossi M, Pierron F. Identification of plastic constitutive parameters at large deformations from three dimensional displacement fields. Comput Mech 2012;49(1):53–71. doi:10.1007/s00466-011-0627-0.

[20] Rossi M, Pierron F, Štamborská M. Application of the virtual fields method to large strain anisotropic plasticity. Int J Solids Struct 2016;97–98:322–35. doi:10.1016/j.ijsolstr.2016.07.015.

[21] Dunne F, Petrinic N. Introduction to computational plasticity. Oxford University Press on Demand; 2005.

[22] Lecompte D, Smits A, Sol H, Vantomme J, Van Hemelrijck D. Mixed numerical–experimental technique for orthotropic parameter identification using biaxial tensile tests on cruciform specimens. Int J Solids Struct 2007;44(5):1643–56. doi:10.1016/j.ijsolstr.2006.06.050.

[23] Bruno L, Felice G, Pagnotta L, Poggialini A, Stigliano G. Elastic characterization of orthotropic plates of any shape via static testing. Int J Solids Struct 2008;45(3):908–20. doi:10.1016/j.ijsolstr.2007.09.017.

[24] Kajberg J, Lindkvist G. Characterisation of materials subjected to large strains by inverse modelling based on in-plane displacement fields. Int J Solids Struct 2004;41(13):3439–59. doi:10.1016/j.ijsolstr.2004.02.021.

[25] Cooreman S, Lecompte D, Sol H, Vantomme J, Debruyne D. Identification of mechanical material behavior through inverse modeling and dic. Exp Mech 2008;48(4):421–33. doi:10.1007/s11340-007-9094-0.

[26] Pottier T, Toussaint F, Vacher P. Contribution of heterogeneous strain field measurements and boundary conditions modelling in inverse identification of material parameters. Eur J Mech A Solids 2011;30(3):373–82. doi:10.1016/j.euromechsol.2010.10.001.

[27] Kajberg J, Wikman B. Viscoplastic parameter estimation by high strain-rate experiments and inverse modelling–speckle measurements and high-speed photography. Int J Solids Struct 2007;44(1):145–64. doi:10.1016/j.ijsolstr.2006.04.018.

[28] Ghouati O, Gelin J-C. A finite element-based identification method for complex metallic material behaviours. Comput Mater Sci 2001;21(1):57–68. doi:10.1016/S0927-0256(00)00215-9.

[29] Cao J, Lin J. A study on formulation of objective functions for determining material models. Int J Mech Sci 2008;50(2):193–204. doi:10.1016/j.ijmecsci.2007.07.003.

[30] Andrade-Campos A, de Carvalho R, Valente R. Novel criteria for determination of material model parameters. Int J Mech Sci 2012;54(1):294–305. doi:10.1016/j.ijmecsci.2011.11.010.

[31] Mathieu F, Leclerc H, Hild F, Roux S. Estimation of elastoplastic parameters via weighted FEMU and integrated-DIC. Exp Mech 2015;55(1):105–19. doi:10.1007/s11340-014-9888-9.

[32] Avril S, Bonnet M, Bretelle A-S, Grédiac M, Hild F, Ienny P, et al. Overview of identification methods of mechanical parameters based on full-field measurements. Exp Mech 2008;48(4):381. doi:10.1007/s11340-008-9148-y.

[33] Denys K, Coppieters S, Cooreman S, Debruyne D. Alternative method for the identification of the strain hardening behaviour along the rolling direction of coil. Strain 2017;53(5) e12231–n/a. doi:10.1111/str.12231.

[34] Fu J, Barlat F, Kim J-H, Pierron F. Application of the virtual fields method to the identification of the homogeneous anisotropic hardening parameters for advanced high strength steels. Int J Plast 2017;93:229–50. doi:10.1016/j.ijplas.2016.07.013. Special Issue on Constitutive Descriptions of Plasticity at Various Scales in memory of Prof. José J. Grácio

[35] Bui H, Constantinescu A. Spatial localization of the error of constitutive law for the identification of defects in elastic bodies. Arch Mech 2000;52(4–5):511–22.

[36] Roux S, Hild F, Pagano S. A stress scale in full-field identification procedures: a diffuse stress gauge. Eur J Mech A Solids 2005;24(3):442–51. doi:10.1016/j.euromechsol.2005.02.002.

[37] Geymonat G, Hild F, Pagano S. Identification of elastic parameters by displacement field measurement. Comptes Rendus Mécanique 2002;330(6):403–8. doi:10.1016/S1631-0721(02)01476-6.

[38] Florentin E, Lubineau G. Identification of the parameters of an elastic material model using the constitutive equation gap method. Comput Mech 2010;46(4):521–31. doi:10.1007/s00466-010-0496-y.

[39] Florentin E, Lubineau G. Using constitutive equation gap method for identification of elastic material parameters: technical insights and illustrations. Int J Interact Des Manuf 2011;5(4):227–34. doi:10.1007/s12008-011-0129-5.

[40] Guchhait S, Banerjee B. Anisotropic linear elastic parameter estimation using error in the constitutive equation functional. Proc R Soc Lond A Math Phys Eng Sci 2016;472(2192). doi:10.1098/rspa.2016.0213.

[41] Latourte F, Chrysochoos A, Pagano S, Wattrisse B. Elastoplastic behavior identification for heterogeneous loadings and materials. Exp Mech 2008;48(4):435–49. doi:10.1007/s11340-007-9088-y.

[42] Merzouki T, Nouri H, Roger F. Direct identification of nonlinear damage behavior of composite materials using the constitutive equation gap method. Int J Mech Sci 2014;89:487–99. doi:10.1016/j.ijmecsci.2014.10.002.

[43] Coppieters S, Kuwabara T. Identification of post-necking hardening phenomena in ductile sheet metal. Exp Mech 2014;54(8):1355–71. doi:10.1007/s11340-014-9900-4.

[44] Crisfield M. Non-Linear finite element analysis of solids and structures, 1. John Wiley & Sons, Ltd.; 1991.

[45] Roux S, Hild F. Digital image mechanical identification (DIMI). Exp Mech 2008;48(4):495–508. doi:10.1007/s11340-007-9103-3.

[46] Périé JN, Leclerc H, Roux S, Hild F. Digital image correlation and biaxial test on composite material for anisotropic damage law identification. Int J Solids Struct 2009;46(11):2388–96. doi:10.1016/j.ijsolstr.2009.01.025.

[47] Amiot F, Périé J-N, Roux S. Equilibrium gap method. John Wiley & Sons, Inc.; 2012. p. 331–62. ISBN 9781118578469. doi:10.1002/9781118578469.ch12.

[48] Pierron F, Grédiac M. The virtual fields method: extracting constitutive mechanical parameters from full-field deformation measurements. Springer Science & Business Media; 2012.

[49] Ma Y, Yao X, Liu X, Hao W, Fang D. Inversion and decoupling of thermo-mechanical deformation in anisotropic materials using the virtual fields method. Proc R Soc Lond A Math Phys Eng Sci 2013;469(2154). doi:10.1098/rspa.2013.0124.

[50] Zhang L, Thakku SG, Beotra MR, Baskaran M, Aung T, Goh JCH, et al. Verification of a virtual fields method to extract the mechanical properties of human optic nerve head tissues *in vivo*. Biomech Model Mechanobiol 2017;16(3):871–87. doi:10.1007/s10237-016-0858-2.

[51] Fu J, Barlat F, Kim J-H, Pierron F. Identification of nonlinear kinematic hardening constitutive model parameters using the virtual fields method for advanced high strength steels. Int J Solids Struct 2016;102:30–43. doi:10.1016/j.ijsolstr.2016.10.020.

[52] Notta-Cuvier D, Langrand B, Lauro F, Markiewicz E. An innovative procedure for characterising a coupled elastoplastic damage model of behaviour using the virtual fields method. Int J Solids Struct 2015;69:415–27. doi:10.1016/j.ijsolstr.2015.05.009.

[53] Notta-Cuvier D, Langrand B, Markiewicz E, Lauro F, Portemont G. Identification of Johnson–Cook's viscoplastic model parameters using the virtual fields method: application to titanium alloy ti6al4v. Strain 2013;49(1):22–45. doi:10.1111/str.12010.

[54] Valeri G, Koohbor B, Kidane A, Sutton MA. Determining the tensile response of materials at high temperature using DIC and the virtual fields method. Opt Lasers Eng 2017;91:53–61. doi:10.1016/j.optlaseng.2016.11.004.

[55] Grediac M, Pierron F, Avril S, Toussaint E. The virtual fields method for extracting constitutive parameters from full-field measurements: a review. Strain 2006;42(4):233–53. doi:10.1111/j.1475-1305.2006.tb01504.x.

[56] Pierron F, Avril S, Tran VT. Extension of the virtual fields method to elasto-plastic material identification with cyclic loads and kinematic hardening. Int J Solids Struct 2010;47(22):2993–3010. doi:10.1016/j.ijsolstr.2010.06.022.

[57] Marek A, Davis FM, Pierron F. Sensitivity-based virtual fields for the non-linear virtual fields method. Comput Mech 2017. doi:10.1007/s00466-017-1411-6.

[58] Louëdec GL, Pierron F, Sutton MA, Siviour C, Reynolds AP. Identification of the dynamic properties of al 5456 FSW welds using the virtual fields method. J. Dyn. Behav. Mater. 2015;1(2):176–90. doi:10.1007/s40870-015-0014-6.

[59] Leem D, Kim JH, Barlat F, Song JH, Lee MG. Identification of dynamic flow stress curves using the virtual fields methods: theoretical feasibility analysis. Met Mater Int 2018;24(2):351–61. doi:10.1007/s12540-018-0024-8.

[60] Avril S, Grédiac M, Pierron F. Sensitivity of the virtual fields method to noisy data. Comput Mech 2004;34(6):439–52. doi:10.1007/s00466-004-0589-6.

[61] Lasdon LS, Waren AD, Jain A, Ratner M. Design and testing of a generalized reduced gradient code for nonlinear programming. ACM Trans. Math. Softw. (TOMS) 1978;4(1):34–50.

[62] Rossi M, Lava P, Pierron F, Debruyne D, Sasso M. Effect of DIC spatial resolution, noise and interpolation error on identification results with the VFM. Strain 2015;51(3):206–22. doi:10.1111/str.12134.

[63] Marquardt DW. An algorithm for least-squares estimation of nonlinear parameters. J. Soc. Ind. Appl. Math. 1963;11(2):431–41. doi:10.1137/0111030.